

Sussex Research

Acetyl-leucine slows disease progression in lysosomal storage disorders

Ecem Kaya, David A Smith, Claire Smith, Lauren Morris, Tatiana Bremova-Ertl, Mario Cortina-Borja, Paul Fineran, Karl J Morten, Joanna Poulton, Barry Boland, John Spencer, Michael Strupp, Frances M Platt

Publication date

20-12-2020

Licence

This work is made available under the [CC BY 4.0](#) licence and should only be used in accordance with that licence. For more information on the specific terms, consult the repository record for this item.

Document Version

Published version

Citation for this work (American Psychological Association 7th edition)

Kaya, E., Smith, D. A., Smith, C., Morris, L., Bremova-Ertl, T., Cortina-Borja, M., Fineran, P., Morten, K. J., Poulton, J., Boland, B., Spencer, J., Strupp, M., & Platt, F. M. (2020). *Acetyl-leucine slows disease progression in lysosomal storage disorders* (Version 2). University of Sussex.
<https://hdl.handle.net/10779/uos.23477582.v2>

Published in

Brain Communications

Link to external publisher version

<https://doi.org/10.1093/braincomms/fcaa148>

Copyright and reuse:

This work was downloaded from Sussex Research Open (SRO). This document is made available in line with publisher policy and may differ from the published version. Please cite the published version where possible. Copyright and all moral rights to the version of the paper presented here belong to the individual author(s) and/or other copyright owners unless otherwise stated. For more information on this work, SRO or to report an issue, you can contact the repository administrators at sro@sussex.ac.uk. Discover more of the University's research at <https://sussex.figshare.com/>

Acetyl-leucine slows disease progression in lysosomal storage disorders

Short title: Acetyl-leucine for lysosomal diseases

Ecem Kaya¹, David A Smith¹, Claire Smith¹, Lauren Morris¹,
Tatiana Bremova-Ertl^{2,6}, Mario Cortina-Borja³, Paul Fineran¹, Karl J Morten⁴, Joanna
Poulton⁴, Barry Boland⁵, John Spencer⁶, Michael Strupp⁷ and Frances M Platt*¹

¹ Department of Pharmacology, University of Oxford, Mansfield Road, Oxford, UK

² Department of Neurology, Inselspital, Bern University Hospital, University of Bern, Bern, Switzerland

³ Population, Policy and Practice Research and Teaching Department, Great Ormond Street Institute of Child Health, University College London

⁴ Nuffield Department of Women's and Reproductive Health, University of Oxford, Oxford, UK

⁵ Dept. of Pharmacology and Therapeutics, Western Gateway Building, College of Medicine and Health, University College Cork, Ireland

⁶ Department of Chemistry, School of Life Sciences, University of Sussex, Brighton, UK

⁷ Department of Neurology and German Center for Vertigo and Balance Disorders, Ludwig Maximilians University, Munich, Germany

* Corresponding Author: Frances M Platt

Email: Frances.platt@pharm.ox.ac.uk

Address: Department of Pharmacology,

University of Oxford,

Mansfield Road,

Oxford OX1 3QT, UK

Tel: 01865 271858

Fax: 01865 271853

© The Author(s) (2020). Published by Oxford University Press on behalf of the Guarantors of Brain.

This is an Open Access article distributed under the terms of the Creative Commons Attribution License

(<http://creativecommons.org/licenses/by/4.0/>), which permits unrestricted reuse, distribution, and reproduction in any medium, provided the original work is properly cited.

Abstract

Acetyl-DL-leucine is a derivative of the branched chain amino acid leucine. In observational clinical studies acetyl-DL-leucine improved symptoms of ataxia, in particular in patients with the lysosomal storage disorder, Niemann-Pick disease type C1. Here, we investigated acetyl-DL-leucine and its enantiomers acetyl-L-leucine and acetyl-D-leucine in symptomatic *Npc1*^{-/-} mice and observed improvement in ataxia with both individual enantiomers and acetyl-DL-leucine. When acetyl-DL-leucine and acetyl-L-leucine were administered pre-symptomatically to *Npc1*^{-/-} mice, both treatments delayed disease progression and extended life span, whereas acetyl-D-leucine did not. These data are consistent with acetyl-L-leucine being the neuroprotective enantiomer. Altered glucose and antioxidant metabolism were implicated as one of the potential mechanisms of action of the L enantiomer in *Npc1*^{-/-} mice. When the standard of care drug miglustat and acetyl-DL-leucine were used in combination significant synergy resulted. In agreement with these pre-clinical data, when Niemann-Pick disease type C1 patients were evaluated after 12 months of acetyl-DL-leucine treatment, rates of disease progression were slowed, with stabilisation or improvement in multiple neurological domains. A beneficial effect of acetyl-DL-leucine on gait was also observed in this study in a mouse model of GM2 gangliosidosis (Sandhoff disease) and in Tay-Sachs and Sandhoff disease patients in individual cases of off-label-use. Taken together, we have identified an unanticipated neuroprotective effect of acetyl-L-leucine and underlying mechanisms of action in lysosomal storage diseases, supporting its further evaluation in clinical trials in lysosomal disorders.

Keywords

Lysosomal storage diseases, Niemann-Pick disease type C, GM2 gangliosidosis, acetyl-leucine, miglustat.

Abbreviations

ADL	Acetyl-D-Leucine
ADLL	Acetyl-DL-Leucine
ADP	Adenosine Diphosphate
ALL	Acetyl-L-Leucine
ASIS	Annual Severity Increment Score
BCAA	Branched chain amino acid
BCKDHA	Branched Chain Keto Acid Dehydrogenase Subunit A
CA	Cerebellar Ataxia
CHO	Chinese Hamster Ovary
CI-CS	Clinical Impression of Change in Severity
GDH	Glutamate Dehydrogenase
GSL	Glycosphingolipid
LDH	Lactate Dehydrogenase
LSD	Lysosomal Storage Diseases
mTOR	Mammalian Target of Rapamycin
NAD	Nicotinamide adenine dinucleotide
NADH	Nicotinamide adenine dinucleotide (reduced form)
NPC1	Niemann-Pick Disease Type C 1
MOA	Mechanism of action
MoCA	Montreal Cognitive Assessment
PDH	Pyruvate Dehydrogenase
PDK	Pyruvate Dehydrogenase Kinase
PDP	Pyruvate Dehydrogenase Phosphatase
PGC-1alpha	Peroxisome Proliferator-activated Receptor-gamma Coactivator 1-alpha
ROS	Reactive Oxygen Species
SOD	Superoxide Dismutase
SARA	Scale for Assessment and Rating of Ataxia
8MWT	8-Minute-Walking-Test

Introduction

Acetyl-DL-leucine (ADLL) is a racemic (1:1) mixture of enantiomers and a derivative of the branched chain amino acid (BCAA) leucine. It has been used as a medication (Tanganil™) for the treatment of acute vertigo in France and former French colonies since 1957; it is orally available and has a good safety profile according to the Periodic Updated Safety Reports from Pierre-Fabre, France. Although its mechanism of action is not fully known, studies in a guinea pig model of acute vertigo showed that ADLL can restore membrane potential and excitability of abnormally polarised neurons of the medial vestibular nucleus (Vibert and Vidal, 2001).

Due to the phylogenetic similarities and close interactions between vestibular and deep cerebellar neurons (Highstein and Holstein, 2005), and an activation of cerebellar neurons is an essential part of central vestibular compensation, the effects of ADLL were evaluated in patients with cerebellar ataxias (CA) who have impaired function of cerebellar neurons. ADLL was shown to be beneficial in patients with CA (Strupp *et al.*, 2013; Schniepp *et al.*, 2016). Since CA is one of the leading clinical symptoms of some lysosomal storage disorder (LSD) such as Niemann-Pick disease type C 1 (NPC1) and the GM2 gangliosidosis (Tay-Sachs and Sandhoff disease), the symptomatic effects of ADLL were examined in 12 patients with NPC1 who were treated with the oral formulation of ADLL for a month (5 g/d). ADLL therapy in NPC1 patients led to significant improvements in CA as well as in cognition and behaviour, suggestive of potential functional benefits beyond the cerebellum (Bremova *et al.*, 2015). Our findings of *in vitro* benefit of ADLL in Tangier disease fibroblasts (Colaco *et al.*, 2019), and *in vivo* slowing disease progression in Sandhoff disease mice (Kaya *et al.*, 2020) suggest ADLL may have the potential for therapeutic use in a broader range of diseases.

In all of these studies, ADLL was administered to patients as a racemic mixture of acetyl-D-leucine (ADL) and acetyl-L-leucine (ALL) enantiomers. Pre-clinical studies implicated ALL as the active isomer responsible for postural compensation after unilateral vestibular damage in an animal model (Günther *et al.*, 2015; Tighilet *et al.*, 2015), and three clinical trials are ongoing with acetyl-L-leucine: NPC, GM2 gangliosidosis and ataxia telangiectasia (clinicaltrials.gov NCT03759639, NCT03759665, NCT03759678). CNS exposure of the administered compounds is equivalent within the limitations of the methods used, but L is metabolized rapidly whereas D is inert (Churchill *et al.*, 2020). However, it remains to be determined if this proposed mechanism of action is relevant to the effects of ADLL and individual enantiomers in NPC.

In the current study, we have therefore investigated the efficacy of ADLL and its distinct enantiomer components in a mouse model of NPC1 (*Npc1*^{-/-}). We found that ADLL and its enantiomers significantly improved ataxia in *Npc1*^{-/-} mice, in agreement with clinical observations with ADLL (Bremova *et al.*, 2015). It is important to note, when administered pre-symptomatically ADLL (50% ALL: 50% ADL) and ALL, but not ADL, slowed the rate of disease progression, were neuroprotective, and significantly extended lifespan. Therefore, pre-clinical studies implicate ALL as the active enantiomer of ADLL responsible for the neuroprotective effects of the treatment.

When miglustat, the currently approved therapy for NPC1 (Patterson *et al.*, 2007), was combined with ADLL in *Npc1*^{-/-} mice, significant synergistic benefit resulted, including further extension of life span. In a cohort of NPC1 patients, the significant neuroprotective effects of ADLL identified in *Npc1*^{-/-} mice were also observed in a 12-18-month extension phase of an ongoing observational study (Cortina-Borja *et al.*, 2018). When the mechanism of action of ADLL and its enantiomers were investigated in the cerebellum of treated *Npc1*^{-/-} mice, modulation of pathways involved in glucose metabolism were identified as potentially

mediating the beneficial effects of the L-enantiomer. Finally, in individual-cases of off-label-use ADLL improved function in three GM2 gangliosidosis patients (Tay-Sachs and Sandhoff disease) and gait improvements were also demonstrated in a mouse model of Sandhoff disease. These findings demonstrate the distinct benefits of acetyl leucine treatments in LSDs and show promise for clinical applications.

Materials and Methods

Animals and treatments. BALBc/NPC1^{nih} (Pentchev *et al.*, 1980) and Sandhoff (*Hexb*^{-/-}) mice (Sango *et al.*, 1995) were bred as heterozygotes to generate homozygous null (*Npc1*^{-/-}) and mutant (*Hexb*^{-/-}) mice, along with their respective wild-type controls (*Npc1*^{+/+}, *Hexb*^{+/+}). Mice were housed under non-sterile conditions, with food and water available *ad libitum*. Since the phenotypic development affects both genders similarly upon *Npc1* abrogation (Morris *et al.*, 1982), all experiments were conducted on female mice to facilitate group housing from different litters using protocols approved by the UK Home Office Animal Scientific Procedures Act, 1986. All animal works was conducted under the UK Home Office licensing authority and the Project licence number is P8088558D. Mice were randomly assigned to treatment groups and the drugs coded and the staff blinded to treatment when performing behavioural analysis.

Chinese hamster ovary cells. Wild-type and NPC1 deficient CHO cells were used for *in vitro* experiments and have been described previously (Dahl *et al.*, 1992; Higaki *et al.*, 2001)

Drug treatments. Acetyl leucine analogues (ALs) and miglustat treatment protocols are described in the **supplemental experimental procedures**.

Mouse behavioural analysis. The weight and activity of each mouse was recorded weekly until reaching the humane endpoint (defined as a loss of 1g body weight within 24h). CatWalk (10.5 system (Noldus)), NG Rota Rod for mice (Ugo Basile) was performed as described in the **supplemental experimental procedures**.

Biochemical and immunohistochemical analyses

Sample preparation. Mice were saline perfused under terminal anaesthesia. Tissues for biochemical analysis were snap-frozen on ice-cold isopentane. For immunofluorescent staining, tissues were perfused with 4% PFA followed by PBS and kept in 4% PFA for 24h then stored in PBS containing 20% w/v sucrose. Biochemical analyses were performed on water-homogenised tissues (50 mg/mL) and protein content determined (BCA protein assay, Thermo Fisher #23227) according to the manufacturer's instructions.

Western blot analyses. Western blot analyses were performed on mouse cerebellum as described in the **supplemental experimental procedures**.

ADP and ATP extraction. ADP and ATP were extracted with Phenol-TE from 70-150 mg tissues according to published methods (Chida *et al.*, 2012). For details, see **supplemental experimental procedures**.

NAD and NADH extraction. NAD and NADH extractions were performed on 20 mg PBS washed fresh tissue on wet ice homogenised with a Dounce homogeniser with 400uL of NADH/NAD extraction buffer (Abcam NAD/NADH Assay kit-ab65348). For details, see **supplemental experimental procedures**.

Sample analysis

Sphingoid Base Measurements. Sphingoid base extraction and detection with reverse phase HPLC was performed as described in the **supplemental experimental procedures**.

Glycosphingolipid measurements. Glycosphingolipids were extracted and measured by Normal Phase-HPLC according to published methods (Neville *et. al.*, 2004). For details, see **supplemental experimental procedures.**

Cholesterol measurements. Cholesterol was measured from Folch-extracted tissues with the Amplex Red kit (Molecular Probes) according to the manufacturer's instructions. For details, refer to **supplemental experimental procedures.**

Flow cytometry experiments of CHO cells. Relative acidic compartment volume staining of live cells was with LysoTracker™ Green DND-26 (Thermo Fisher-L7526), mitochondrial volume was determined with MitoTracker Green (Invitrogen #M7514) and mitochondrial reactive oxygen species with MitoSOX Red (Invitrogen #M36008). For details, refer to **supplemental experimental procedures.**

Filipin Staining of CHO cells. Free unesterified cholesterol was visualized in CHO cells grown on glass coverslips using filipin labelling (from *Streptomyces filipinensis* (Sigma)). For details, refer to **supplemental experimental procedures.**

Immunohistochemistry. Immunohistochemistry was performed as described in the **supplemental experimental procedures.** The antibodies used are summarised in **Supplementary Table 1.** Slides were air dried and mounted in ProLong Gold antifade (Invitrogen, #P36930).

Western Blotting. Western blotting was performed as described in **supplemental experimental procedures.** The antibodies used are summarised in **Supplementary Table 1.**

Image Acquisition and Quantification. Imaging of brain sections and CHO cells was performed with a Leica-SP8 confocal microscope. Western blot data acquisition was conducted with LiCOR Odyssey Infrared imaging system (Model No. 9120) and Universal hood II (Bio-Rad, California, USA). Mean fluorescence values, cerebellum diameters and areas, and cell quantifications were calculated with Fiji Version 1.51g software (Image J) (<http://fiji.sc/Fiji>) (W. Rasband, NIH, USA). See **supplemental experimental procedures** for analysis of cerebellar sections.

ADP/ATP measurements. Measurements of ADP/ATP were made using a kit from Sigma Aldrich (Cat#: MAK135) according to the manufacturer's instructions. The ADP/ATP ratio was calculated with the equation: $(RLU-C-RLUB)/RLU-A$.

NAD, NADH measurements. NAD, NADH and total NAD (NADt) ($NAD+NADH=NADt$) were measured with the NAD/NADH assay kit (Abcam-ab65348). For details, refer to **supplemental experimental procedures**.

Clinical Studies

Demographics and statistical analysis of individual-cases of off-label-use of adult NPC1 patients treated with ADLL is described in the **supplemental experimental procedures**.

Individual-cases of off-label-use in GM2 gangliosidosis patients are described in the **supplemental experimental procedures**.

Blinded Video-Rating is described in the **supplemental experimental procedures**.

All patients gave their informed consent according to the Declaration of Helsinki prior to the compassionate use study.

Statistical analysis and Power calculations

To calculate the number of mice needed for the experimental groups in this study we used G*Power software (<http://www.gpower.hhu.de>). The power was set as 0.8 and the significance level, α , as 0.05. The mean lifespan of the NPC1 mouse model in our facility is 87 days with a standard deviation of 3 days. NPC1 is a disease with no curative treatment and many experimental disease-modifying drugs have reported a 10-30% increase in lifespan. Therefore, we based our power calculation on a 10-30% effect size and a sample size of min 5 and max 8 animals per group was determined. For statistical analysis see **supplemental experimental procedures**.

Data availability

Data will be made available upon reasonable request.

Results

ADLL, ALL and ADL administered during the symptomatic phase of disease improves ataxia in *Npc1*^{-/-} mice.

Npc1^{-/-} mice have a 10-12-week life span, with onset of symptoms (gait abnormalities, tremor and weight loss) beginning at 6-7 weeks of age (Williams *et al.*, 2014). ADLL, ALL and ADL were administered to *Npc1*^{-/-} mice in their diet (0.1 g/kg/day), with a dose identical to that used in observational clinical studies (Bremova *et al.*, 2015). Untreated 9-week-old *Npc1*^{-/-} mice exhibit statistically significant ataxia that presents as a pronounced sigmoidal gait, relative to wild-type mice ($p < 0.0001$) (**Supplementary Figure 1**), whereas 9-week-old *Npc1*^{-/-} mice treated with ADLL, ALL or ADL from 8-weeks of age (1 week of treatment) all displayed significantly reduced ataxia as determined by measuring lateral displacement from a straight trajectory in an automated gait analysis system (**Supplementary Figure 1**) (**Figure 1a and b**) ($p < 0.0001$, all treatments). These results indicate that the acute anti-ataxic effect of acetyl-leucine is stereoisomer-independent in *Npc1*^{-/-} mice.

Pre-symptomatic treatment with ADLL, ALL and ADL improves ataxia in *Npc1*^{-/-} mice.

We investigated whether any additional benefit was conferred by AL analogues if treatment commenced before symptom onset. *Npc1*^{-/-} mice were therefore treated pre-symptomatically from weaning (3 weeks of age) and assessed at 9 weeks of age (6 weeks of treatment). Similar to the acute treatment response, all three AL analogues tested significantly reduced ataxia (**Figure 1a and c**) ($p < 0.0001$ for all treatments) with the magnitude comparable to the effects observed with one week of treatment (**Figure 1a and Supplementary Figure 1**).

Pre-symptomatic treatment with ADLL and ALL, but not ADL, improves gait abnormalities, motor function and modestly extends survival in $Npc1^{-/-}$ mice.

$Npc1^{-/-}$ mice develop motor dysfunction (measured by Rotarod) and paw placement abnormalities when ambulatory (measured with CatWalk). We therefore treated $Npc1^{-/-}$ mice pre-symptomatically from weaning (3 weeks of age) and assessed the mice at 8 weeks of age. Untreated $Npc1^{-/-}$ mice had a significantly improved hind paw duty cycle (**Figure 1d**, $p=0.0031$) and an improved hind paw stand mean ($p=0.0026$) relative to wild-type mice (Kirkegaard *et al.*, 2016) (**Figure 1e**). Pre-symptomatic ADLL and ALL treatment of $Npc1^{-/-}$ mice resulted in a functional improvement in duty cycle of hind paws (ADLL: $p=0.0005$, ALL: $p<0.0001$) (**Figure 1d**) and hind paw stand mean (ADLL: $p=0.0179$, ALL: $p=0.0014$) relative to untreated $Npc1^{-/-}$ mice (**Figure 1e**). Rotarod performance was significantly impaired in untreated $Npc1^{-/-}$ mice relative to wild-type littermates ($p<0.0001$) (**Figure 1f**). Treatment with ADLL ($p=0.0088$) and ALL ($p=0.0070$) resulted in a significant improvement in Rotarod performance by $Npc1^{-/-}$ mice (**Figure 1f**). ADL treatment had no significant benefit on $Npc1^{-/-}$ mouse motor function, as assessed using Catwalk (hind paw duty cycle $p=0.2124$, hind paw stand mean $p=0.9547$) or Rotarod ($p=0.2218$) (**Figure 1d-f**). Relative to untreated $Npc1^{-/-}$ mice, the life span of animals treated from weaning was modestly but significantly increased by 8 days (9.1%) with ALL treatment ($p=0.0334$), 4 days with ADLL ($p=0.0305$) (4.5%) and was not changed with ADL ($p=0.6908$) (**Figure 1g**), therefore displaying L-enantiomer selectivity.

ADLL, ALL and ADL improve neuropathology and reduce some lipid species in $Npc1^{-/-}$ mouse brain in a stereo-selective manner.

Since NPC1 disease is characterized by the accumulation of sphingoid bases (sphingosine and sphinganine), cholesterol, sphingomyelin, free fatty acids and glycosphingolipids (GSLs) (Lloyd-Evans and Platt, 2010) we measured the impact of ALs administered to $Npc1^{-/-}$ mice

from 3 weeks of age on lipid storage in the brain. At 59 days of age *Npc1*^{-/-} mice exhibited increased lipid levels relative to wild-type (Williams *et al.*, 2014) (**Figure 2a-f**). In order to evaluate the differential impact of the AL analogues in the CNS we analyzed the cerebellum and the forebrain (referred to as brain in the **Figure 2**) separately. Total GSLs in the forebrain were not significantly altered by any of the AL treatments (**Supplementary Figure 2a**), whilst ALL selectively reduced GM1a (20.1%; $p= 0.0018$) and GM2 (19.6%; $p= 0.0222$) (**Figure 2a**). Interestingly, although sphingosine levels were not significantly affected, ADLL and ADL reduced sphinganine levels by 13.5% ($p= 0.0456$) and 18.2% ($p= 0.0111$) respectively (**Figure 2b and c**). Analysis of the cerebellum confirmed no significant difference in total GSLs relative to untreated *Npc1*^{-/-} mice with any of the AL analogues tested (**Supplementary Figure 2b**). However, ADLL and ALL treatment significantly lowered levels of specific GSLs including GA2 (ADLL: 21.3%, $p= 0.0102$; ALL: 23.8%, $p= 0.0042$), whereas a significant reduction in GA1 was only observed with ALL treatment (23.5%, $p= 0.0254$) (**Figure 2d**). Sphingosine levels were increased by 19%, ($p= 0.0042$), but sphinganine was significantly reduced following ADL treatment (42.3%, $p= 0.0074$) (**Figure 2e and f**). These results indicate differential biological targets of the two enantiomers. Cholesterol levels in the forebrain and in the cerebellum were not shown as total brain cholesterol levels are not changed in the NPC brain (Xie *et al.*, 2000).

ADLL slows Purkinje cell loss and ALL reduces neuroinflammation in the cerebellum, whereas ADL has no neuroprotective effect.

Npc1^{-/-} mice exhibit progressive neurodegeneration, with cerebellar Purkinje neuron loss progressing from anterior to posterior lobes, accompanied by microglial activation (Williams *et al.*, 2014) (**Figure 2g**). Only ADLL treatment significantly increased Purkinje cell survival at 59 days of age relative to untreated *Npc1*^{-/-} littermates: 133% more Purkinje cells were present in lobules I and II ($p= 0.0027$), and 402% more Purkinje cells in lobule III ($p=$

0.0108) (**Figure 2g and h**). Other treatments did not significantly improve Purkinje cell survival in any cerebellar lobules (*Npc1*^{-/-}ALL lobule I-II $p= 0.107$, lobule III $p= 0.157$, lobule IV-V $p= 0.533$; *Npc1*^{-/-}ADL lobule I-II $p= 0.60$, lobule III $p= 0.11$, lobule IV-V $p= 0.766$, compared to *Npc1*^{-/-} UT) (**Figure 2g and h**). However, it is important to note that all of the *Npc1*^{-/-} experimental groups (untreated-treated) possessed 5 to 10 times lower numbers of Purkinje cells in their cerebellum compared to wild-type mice (**Supplementary Figure 2c**). In addition, only ALL treatment significantly reduced (by 20%, $p= 0.0177$) the frequency of CD68-positive activated microglia (**Figure 2g and i**) while other treatments did not have a significant impact ($p= 0.1353$ for *Npc1*^{-/-}ADLL, $p= 0.0553$ for *Npc1*^{-/-}ADL compared to *Npc1*^{-/-} UT). ADL did not mediate any long term, neuroprotective effects assessed with Purkinje cell count and CD68 staining. Lastly, we measured myelin basic protein levels in the cerebellum by western blotting, and saw no changes in myelin basic protein content with AL treatments (**Supplementary Figure 2d and e**).

All AL treatments alleviate lipid storage in non-neuronal tissues and cells.

Liver GSL levels in the *Npc1*^{-/-} mice were significantly reduced in *Npc1*^{-/-} mice treated with ADLL (26.8%, $p= 0.03$), ADL (26.9%, $p= 0.0253$) and 45.5% for ALL ($p= 0.0003$) (**Supplementary Figure 2f**). Quantification of the major GSL species confirmed that levels of GM2Gc (the most abundant GSL in the mouse liver) was decreased significantly with all AL analogues tested (26.7% ADLL: $p= 0.0002$, 45% ALL: $p< 0.0001$, 29% ADL: $p< 0.0001$), while GM3Gc levels were only reduced significantly by ALL (54.8%: $p= 0.0314$) relative to untreated *Npc1*^{-/-} mice (**Figure 3a**). All analogues tested caused significant and comparable levels of reduction of sphingosine (the catabolic break down product of ceramide) (ADLL 29.5%, $p= 0.0233$; ALL 33.2%, $p= 0.0148$; ADL 33.6% $p= 0.0103$) and its *de novo* precursor sphinganine (ADLL 32.5% $p= 0.0365$; ALL 37.4% $p= 0.0189$; ADL 38.5% $p= 0.0163$) (**Figure 3b and c**). Total free cholesterol in *Npc1*^{-/-} liver was also

significantly decreased after treatment with ADLL, ALL or ADL (ADLL 18.2% $p= 0.0346$; ALL 23.4% $p= 0.0091$; ADL 16.2 % $p= 0.0210$) (**Figure 3d**).

Reduction of lipid species in the liver with all three AL treatments led us to investigate whether other non-neuronal cell types were corrected by ALs. We conducted a series of experiments on NPC1 deficient Chinese Hamster Ovary (CHO) cells by utilizing lysosomal and mitochondrial probes as well as measurements of lipid storage. NPC1 protein deletion/mutation results in increased lysosomal volume (Te Vruchte *et al.*, 2014), as well as an increase in mitochondria (measured by MitoTracker), mitochondrial superoxide increase (measured by MitoSOX) (Paulina Ordonez *et al.*, 2012). CHO cells treated with 1mM ALs for 24 hours resulted in normalisation of MitoSOX staining with all three drugs ($p < 0.0001$, compared to NPC1 UT) (**Figure 3e and Supplementary Figure 3**), and a significant decrease in MitoTracker Green (ADLL 16.8% $p= 0.0150$; ALL 17.1% $p= 0.0133$; ADL 15.8% $p= 0.0215$) (**Figure 3e and Supplementary Figure 3**). We found that only 1mM ADLL and ALL treatment reduced relative lysosomal volume after 24h (ADLL 16.9%, $p= 0.0137$; ALL 16%, $p= 0.0177$) (**Figure 3e and Supplementary Figure 3**); however, this beneficial effect was seen with all three acetyl leucine treatments after 72h of treatment (ADLL 24% $p= 0.0026$; ALL 22.8% $p= 0.0036$; ADL 22.3 % $p= 0.0042$) (**Figure 3e and Supplementary Figure 3**). After 72 hr AL treatment, sphingosine levels were significantly reduced by 22% with ADLL ($p= 0.0009$), 29% with ALL ($p < 0.0001$) and 14% with ADL ($p= 0.0149$) (**Figure 3f**). Total GSL levels were significantly reduced with all treatments (26% with ADLL $p= 0.0007$; 25% with ALL $p= 0.0010$; and 22% with ADL $p= 0.0024$) (**Figure 3f**). Likewise, cholesterol content was significantly reduced (18% with ADLL $p= 0.0043$; 13% with ALL $p= 0.0263$; and 14% with ADL $p= 0.0212$) (**Figure 3f, g**).

ADLL synergises with miglustat in *Npc1*^{-/-} mice.

We treated *Npc1*^{-/-} mice with ADLL in combination with the standard of care drug miglustat (600mg/kg/day), resulting in a statistically significant longer life span than animals on monotherapy (*Npc1*^{-/-} miglustat vs *Npc1*^{-/-} miglustat & ADLL $p= 0.0016$; *Npc1*^{-/-} ADLL vs *Npc1*^{-/-} miglustat & ADLL $p= 0.0063$; median survivals; *Npc1*^{-/-} UT: 87 days, *Npc1*^{-/-} ADLL: 91 days; *Npc1*^{-/-} miglustat: 117 days, *Npc1*^{-/-} miglustat & ADLL: 138 days) (**Figure 4a**). Miglustat is known to cause weight loss through appetite suppression (Priestman *et al.*, 2008). When ADLL was used in combination with miglustat it prevented the weight loss associated with miglustat treatment (**Figure 4b**) but not the weight loss resulting from progression of the disease. Combination therapy significantly increased Rotarod performance (8 weeks: $p= 0.0007$; 10,12 weeks $p< 0.0001$ versus untreated *Npc1*^{-/-}), with combination therapy associated with increased benefit relative to mice receiving either miglustat (10 weeks: $p= 0.0299$; 12 weeks: $p= 0.0232$) or ADLL monotherapy (10,12 weeks: $p< 0.0001$) (**Figure 4c**). Gait analysis at 10 weeks of age demonstrated that hind Duty Cycle percentages were significantly improved with combination therapy ($p= 0.0028$) whereas miglustat monotherapy showed no benefit (**Figure 4d and e**). Stand mean significantly improved in mice treated either with combination therapy ($p= 0.0250$) or miglustat monotherapy ($p= 0.0196$) (**Figure 4d, f**). Due to limited availability of miglustat, ALL and ADL combination therapies were not evaluated.

Potential targets of Leucine analogues in the cerebellum

We investigated the potential targets that ALs could affect in the cerebellum since this brain region is particularly important in NPC1-related pathology. As L-Leucine is a potent activator of the mammalian target of rapamycin (mTOR) (Kimball *et al.*, 1999), which negatively regulates autophagy (Klionsky and Emr, 2000), we investigated mTOR and its phosphorylation status in the cerebellum of AL treated *Npc1*^{-/-} mice. Western blotting

indicated that levels of mTOR and its phosphorylation on serine 2448 (Yanagisawa *et al.*, 2017) (phosphorylated/total protein expression ratios (p/t)) were not changed by ADLL, ALL or ADL (**Figure 5a and d**). Autophagic vacuoles accumulate in NPC1 disease, consistent with impaired lysosomal flux (Boland *et al.*, 2010). None of the compounds significantly changed the ratio of LC3-I and LC3-II (**Figure 5b and d**). Furthermore, none of the ALs changed autophagic function or flux (**Figure 5b and d**). In addition, we were unable to detect a significant change in levels of its substrate p62/SQSTM1 (Pankiv *et al.*, 2007) (**Figure 5c and d**).

Effects on energy metabolism and anti-oxidant pathways

In order to investigate potential disruption of branched chain amino acid metabolism we examined mitochondrial branched chain keto acid dehydrogenase enzyme A subunit (BCKDHA), which functions in the final step of the pathway that yields acetyl CoA (Harris *et al.*, 2005). Phosphorylation of BCKDHA (that inactivates the enzyme) was significantly reduced in untreated *Npc1*^{-/-} cerebellum relative to wild type (37.6%, $p=0.0254$) and the ratio of phosphorylated enzyme (p) and total enzyme (t)-p/t was significantly increased (36.6%, $p=0.0269$) (**Figure 5e and f**) in *Npc1*^{-/-} cerebellum. None of the ALs tested had a significant impact on either total BCKDHA levels or the extent of its phosphorylation (**Figure 5e and f**). Branched chain amino acids, especially leucine, are important for glutamine/glutamate balance and for energy metabolism when glucose metabolism is deficient or impaired (Yudkoff, 1997)(Kennedy *et al.*, 2016). However, there was no difference in mitochondrial enzyme glutamate dehydrogenase (GDH) protein levels between untreated *Npc1*^{-/-} and *Npc1*^{+/+} mice or following AL treatments (**Figure 5f and g**).

The ratio of nicotinamide adenine dinucleotide and its reduced form (NAD/NADH) regulates various metabolic pathway enzymes, such as those involved in glycolysis and the TCA cycle (including pyruvate dehydrogenase enzyme) (Srivastava, 2016). NAD/NADH

production (mostly derived from the TCA cycle) fuels the mitochondrial respiratory chain and therefore is of high importance in energy metabolism (Da Veiga Moreira *et al.*, 2015). We therefore measured the changes in NAD/NADH content in the cerebellum and their ratio upon AL treatments. NAD and NADH were decreased in *Npc1*^{-/-} relative to *Npc1*^{+/+} mice achieving statistical significance for NADH (55.1%, $p= 0.0314$) and the sum of NAD and NADH (49.2%, $p= 0.0001$) (**Figure 6a**). Although there was no change in the levels of the coenzymes following AL treatments, in comparison with untreated NPC1 and WT (**Figure 6a**), the NAD/NADH ratio was significantly decreased with ADLL treatment (30.7%, $p= 0.0240$) (**Figure 6b**), which might be an indication of active TCA cycle machinery and glycolysis. The status of energy metabolism also can be assessed by determining adenosine diphosphate and adenosine triphosphate ratio (ADP/ATP). ADP/ATP ratio was also increased with ADLL (**Figure 6c**) ($p= 0.0101$), which might indicate increased energy expenditure and a glycolytic state.

ADLL increases active pyruvate dehydrogenase (PDH) levels while ALL shifts glucose metabolism towards PDH from lactate dehydrogenase (LDH).

We then investigated the effect of AL analogues on glucose utilization that yields NAD (via lactate production) or NADH (via TCA cycle), by measuring levels of pyruvate dehydrogenase (PDH) and lactate dehydrogenase (LDH) proteins by western blotting (**Figure 6 d-h**). PDH is composed of 3 subunits: E1-3, with the active site located on the alpha subunit of E1. Phosphorylation of the E-1 alpha subunit inactivates the PDH enzyme (Kato *et al.*, 2008). Untreated *Npc1*^{-/-} mice at 59 days of age showed significantly decreased levels of PDH-E1 alpha (40.2%, $p= 0.0009$), PDH-E1 beta (61.2%, $p< 0.0001$), PDH-E3 binding protein (PDH-E3bp) (42.2%, $p= 0.0005$) (**Figure 6d and e**), while phospho-PDH (inactive form) (41.4%, $p= 0.0092$), pPDH/PDH E1alpha ratio (55.5%, $p= 0.0006$) and LDH increased in the disease group (14.2%, $p= 0.0335$) (**Figure 6d, f and g**), in comparison to WT.

Accordingly, the glucose metabolism preference (PDHE1 alpha/LDH) favored LDH dependency in untreated *Npc1*^{-/-} mice (74.2%, $p=0.0060$) with no detectable difference in proliferator-activated receptor-gamma coactivator 1-alpha levels (**Figure 6 d-i**). E1 alpha subunit protein levels in PDHC were significantly increased by ADLL (29.1%, $p=0.0146$), ALL (43.3%, $p=0.0004$) and ADL (34.17%, $p=0.0044$) in the cerebellum from treated *Npc1*^{-/-} mice (**Figure 6d and e**), with no changes in E1 beta, E2 or E3bp. The protein levels of phosphorylated E1 alpha subunit were not significantly different following treatment compared to untreated *Npc1*^{-/-} mice. However, the ratio of phosphorylated E1 alpha to total E1 alpha subunit was reduced with ADLL (33%, $p=0.0333$) (**Figure 6d and f**). LDH levels were the same in untreated and treated *Npc1*^{-/-} mice (**Figure 6d and g**). Nevertheless, the ratio of E1 alpha subunit to LDH was significantly shifted in favor of PDH by ALL (49.1%, $p=0.0494$) (**Figure 6h**). Finally, we measured the protein levels of PGC-1 alpha (peroxisome proliferator-activated receptor-gamma coactivator 1-alpha), a key regulator of oxidative phosphorylation (Huiyun and Walter, 2006), to determine whether this metabolic activation and shift towards PDH dependency correlates with changes in oxidative phosphorylation. There was no difference in protein levels of PGC-1 alpha between WT and NPC1 cerebellum or associated with AL treatments (**Figure 6d and i**).

ADLL decreases pyruvate dehydrogenase kinase 2 (PDK2) protein expression.

Pyruvate dehydrogenase is phosphorylated and inactivated by pyruvate dehydrogenase kinase (PDK), reducing flux through the Krebs cycle. In contrast, pyruvate dehydrogenase phosphatase (PDP) dephosphorylates and activates PDH, increasing flux through the Krebs cycle (Jha *et al.*, 2012). We therefore analyzed the expression of three PDK isoforms (PDK1, PDK2 and PDK4) and a single isoform of PDP (PDP1) in the cerebellum (Jha *et al.*, 2012). Whilst levels of PDK1 and PDK4 in the cerebellum were not significantly different between 59-day old *Npc1*^{-/-} and *Npc1*^{+/+} mice, PDK2 was significantly lower (64.4% reduction

compared to wild type, $p < 0.0001$) (**Figure 6j and k**). Furthermore, ADLL (which decreased the phosphorylation of PDH to the greatest extent) decreased PDK2 to a significantly greater extent relative to *Npc1*^{-/-} UT group (42.3%, $p = 0.0022$) (**Figure 6j and k**). PDP1 was unaltered in untreated *Npc1*^{-/-} cerebellum and was only significantly increased by ADL (27.4%, $p = 0.0433$) (**Figure 6j and k**).

Differential effects of individual enantiomers on antioxidant systems: ALL decreases superoxide dismutase (SOD) 1 while ADL increases SOD2.

We assessed the impact of ALs on the anti-oxidative system by measuring the cytoplasmic superoxide dismutase 1 (SOD1) and the mitochondrial superoxide detoxifier superoxide dismutase 2 (SOD2). We were unable to detect any significant difference in SOD1 protein levels between *Npc1*^{-/-} and *Npc1*^{+/+} cerebella but observed a significant reduction in SOD2 (25% $p = 0.0061$) (**Figure 6l and m**). We found that only ALL significantly decreased SOD1 levels in cerebellum (15.6%, $p = 0.0472$) and only ADL significantly elevated SOD2 levels when compared to untreated *Npc1*^{-/-} mice (19.8%, $p = 0.0214$) (**Figure 6l and m**).

Neuroprotective effects of ADLL in individual-cases of off-label-use in NPC1 patients.

Having observed unanticipated beneficial effects of ALs in *Npc1*^{-/-} mice we investigated whether neuroprotective effects also occurred in NPC1 patients treated with ADLL enrolled in an observational clinical study (Cortina-Borja *et al.*, 2018) (for demographics of patients see **Supplementary Table 2**). Total clinical severity scores (with higher values equating to increasing levels of disability (Yanjanin *et al.*, 2010)) were plotted prior to initiation of treatment with Tanganil™ (ADLL), incorporating available retrospective data (**Figure 7a**). All 13 patients had positive slopes of disease progression before ADLL treatment (1.8 severity units/year was the average slope). Following initiation of ADLL treatment the

average slope was -1.78 (3 patients had no slope, 10 had negative slopes) equating to a significant reduction in disease progression and improvement in the majority of patients (One-sided sign test $p= 0.0002$) (**Figure 7a**). The data were also computed as Annual Severity Increment Scores (Cortina-Borja *et al.*, 2018) that measures the rate of disease progression. A mean of -9.1% / year ($p< 0.001$) in ASIS scores was observed (**Figure 7b**). When the slope each patient's pre-treatment total severity score per year was plotted, all patients had positive slopes, whereas post treatment slopes were either zero or negative, consistent with stabilisation or improvement in disease progression (**Figure 7c**). When the treated patient data were analysed by neurological subdomains (**Table 1**) the majority of patients improved or stabilised on treatment in functional and cognitive subdomains (**Table 1**).

ADLL shows benefit in other LSDs: Effects in Sandhoff mice and GM2

gangliosidosis patients

The Sandhoff (*Hexb*^{-/-}) mouse model is pre-symptomatic up to 6-8 weeks of age. Subsequently, they develop tremor and their motor function begins to decline (Jeyakumar *et al.*, 1999). By the later stages of the disease (12-15 weeks) they are inactive and are unable to complete motor function tests such as bar crossing (Jeyakumar *et al.*, 1999). *Hexb*^{-/-} animals were treated from weaning with ADLL (0.1 mg/kg/day, the same dose used for treatment of *Npc1*^{-/-} mice). ADLL-treated mice had improved gait parameters; including hind stand mean ($p=0.0323$) (**Figure 8a**), front ($p= 0.0039$) and hind step cycle ($p= 0.0062$) (**Figure 8b**). To date, ALL and ADL have not been evaluated in the Sandhoff mouse model.

Our findings in Sandhoff mice were extended to individual-cases of off-label-use in three patients with a confirmed GM2 gangliosidosis diagnosis (2 Tay-Sachs and 1 Sandhoff disease (the latter case in press (Bremova-Ertl *et al.*, 2020)) treated with ADLL. We found a mean improvement of the Scale for Assessment and Rating of Ataxia (SARA) by 20.3%, the

Montreal Cognitive Assessment (MoCA) by 17.8% and the 8-M-Walking-Test (8 MWT) by 42%, as shown in **Figure 8c**. All patients and caregivers also reported a subjective improvement and have continued treatment at the same dosage. Videos of the effect of treatment on gait and postural instability are shown in **Videos 1-2**. In addition, three experienced movement disorder experts performed blinded analysis of the videos, and rated the videos based on the Clinical Impression of Severity (CI-S) (1=normal, not at all ill; 2=borderline ill; 3=mildly ill; 4=moderately ill; 5=markedly ill; 6=severely ill; 7=among the most extremely ill). The unbiased observation before and after ADLL treatment showed statistically significant improvements on overall scoring (t-test $p= 0.0039$) (**Figure 8d and Table 2**). ALL and ADL have not been evaluated in clinical settings, but trials with ALL are being conducted (NPC (NCT03759639) and GM2 gangliosidosis (NCT03759665) and Ataxia-Telangiectasia (NCT03759678)).

Discussion

In this study, we have investigated the effects of acetyl-leucine in mouse models of NPC1 and Sandhoff disease and in patients to better understand its therapeutic potential and to gain insights into its mechanism of action (MOA).

We found that ADLL, ALL and ADL significantly improved ataxia when symptomatic *Npc1*^{-/-} mice were treated acutely for seven days; this is in agreement with observational studies in NPC1 patients (Bremova *et al.*, 2015) treated with ADLL, using the same dosage per kg and day. The individual enantiomers provided similar benefit to the racemic mixture for the symptomatic treatment of ataxia. The MOA explaining how ADLL and the enantiomers improve symptoms remains unknown. All AL analogues tested reduced lipid storage in neuronal and non-neuronal tissues in *Npc1*^{-/-} mice and in CHO cells null for *NPC1* suggesting a MOA that is not confined to neuronal cells. The AL analogues were also observed to differentially reduce the levels of stored lipids in the liver and, to a lesser extent, in the brain of treated *Npc1*^{-/-} mice. The mechanism that underpins this “substrate reduction” action of ALs currently remains unclear, but in view of the high degree of synergy when combined with the substrate reduction therapy drug miglustat, it may not be a major contributor to AL’s therapeutic effect in NPC1 disease.

Another major finding of the current study was that ADLL and ALL (but not ADL) slowed disease progression when treatment was initiated before symptom onset, consistent with a neuroprotective mechanism. Since the neuroprotective effects were only observed with ADLL and ALL, this implicated ALL as the active enantiomer and demonstrates that the symptomatic improvement in ataxia and neuroprotection are achieved through different MOA. ALL significantly reduced neuroinflammation, which is important as this actively contributes to disease progression and reducing inflammation using nonsteroidal anti-inflammatory drugs has previously been shown to be beneficial in *Npc1*^{-/-} mice (Williams *et*

al., 2014).

The neuroprotective effect of ADLL and ALL prompted us to determine whether similar effects occur in NPC1 patients treated with ADLL. We took advantage of an ongoing observational study in which thirteen NPC1 patients have been treated with Tanganil™ (ADLL) continuously for approximately 1 year and found that all patients showed stabilisation or improvement in clinical scores which were across all neurological domains, not just those relating to ataxia, supporting a more global neuroprotective effect in patients, analogous to those observed in the *Npc1*^{-/-} mouse.

One central question arising from these studies is the nature of the underlying MOA and in the case of ADLL and ALL, neuroprotective benefit in NPC1. Therefore, we investigated aspects of cell biology and metabolism known to be sensitive to leucine. Leucine has been shown to activate mTOR and reduce LC3-II and p62 in NPC1 cells (Yanagisawa *et al.*, 2017). However, in this study, ADLL, ALL and ADL did not significantly affect either mTOR or autophagy in *Npc1*^{-/-} mouse cerebellum. This might be due to the presence of the acetyl group, as opposed to a primary amine in leucine, blocking the interaction with mTOR, shown in Hela cells (Nagamori *et al.*, 2016) or that acetyl leucine analogues distribute at the cellular level in a manner that prevents their interaction with mTOR. Catabolism of leucine serves as a source of Acetyl-CoA (Harris *et al.*, 1985) which activates mTOR and nutrient sensing pathways (Son *et al.*, 2018). However, the NPC1 cerebellum has significantly decreased levels of acetyl-CoA (Kennedy *et al.*, 2016). This low acetyl-CoA content in NPC1 might therefore prevent nutrient sensing pathway activation. The complexity of mTOR pathways and altered metabolism more generally in NPC1 makes it likely that the effects of AL will likely be context specific.

Altered glucose/energy metabolism has previously been documented in the pre-symptomatic *Npc1*^{-/-} mouse cerebellum (Kennedy *et al.*, 2013). PDHE1 alpha was found to

be inactivated and there was a shift from pyruvate/PDH dependency (upon which neurons rely for aerobic respiration) towards lactate/lactate dehydrogenase (i.e. anaerobic respiration). The consequence of this would be progressive impairment of energy generation (Kennedy *et al.*, 2013). In this same study, alterations in cerebellar amino acids (including leucine), and low acetyl CoA were also reported (Kennedy *et al.*, 2013). Independent metabolomics studies on *Npc1*^{-/-} mouse liver reported imbalances in amino acid levels (Ruiz-Rodado *et al.*, 2016).

In view of data implicating altered energy metabolism in *Npc1*^{-/-} mice, we measured ADP/ATP and NAD/NADH ratios, as a sensitive measure of energy status (Liana Roberts Stein and Imai, 2012; Murphy and Hartley, 2018) and found that ADLL treatment might have shifted the system towards a more TCA-dependent glycolytic state, in the absence of significant changes to NAD-NADH coenzyme levels, (which are lower in *Npc1*^{-/-} cerebellum), in agreement with previous findings in *Npc1*^{-/-} liver (Ruiz-Rodado *et al.*, 2016). We then studied whether the shift in glycolysis is towards pyruvate utilization to produce lactate (anaerobic pathway) or to produce acetyl CoA (aerobic pathway). We found that ADLL treatment significantly increasing PDHE1alpha levels, and decreased PDH enzyme phosphorylation (causes enzyme inactivation) in the cerebellum suggesting activation of the aerobic pathway. Interestingly, PDH-deficient mice also display Purkinje neuron degeneration and relapsing ataxia (Pliss *et al.*, 2013), suggesting the ability of ADLL to protect Purkinje cells against degeneration may be via activation of PDH. However, our findings are based on whole brain lysate and more detailed studies on discrete cell populations would be informative. This effect on PDH did not reflect a change in PGC1-alpha protein levels (indicator of oxidative phosphorylation, OXPHOS), which might be due to the fact that up-regulating OXPHOS requires coenzyme NADH and ADLL treatment does not increase NADH levels.

Individual enantiomers had distinct effects in NPC1 cerebellum; while ALL

normalizes altered levels of PDH and LDH and mildly reduces SOD1 levels, ADL enhanced levels of the mitochondrial reactive oxygen species (ROS) scavenger SOD2 (manganese dependent SOD2). The biological relevance of subtle change in SOD1 level with ALL is unknown and functional readouts are needed to validate this result. *In vivo*, ADLL and ALL treatments were associated with a significantly greater benefit in motor function and lifespan relative to ADL (**Figure 1**). This study suggests that targeting altered cellular metabolism in neurodegenerative diseases may achieve greater efficacy than using antioxidant approaches. The metabolic changes in *Npc1*^{-/-} mice in response to AL treatments are summarized in **Figure 9**.

Finally, we explored whether the benefits of AL are to extend to other LSDs. We observed efficacy of ADLL in a mouse model of Sandhoff disease, one of the GM2 gangliosidoses (Platt *et al.*, 2012), a subgroup of GSL lysosomal storage diseases that includes Tay-Sachs disease: we demonstrated that ADLL treated Sandhoff mice had a significant increase in lifespan and improvements in motor function (Kaya *et al.*, 2020); however the individual isomers ALL and ADL were not assessed. We also found improvement in gait parameters in *Hexb*^{-/-} mice upon ADLL therapy consistent with the observational clinical studies we conducted. In three patients with GM2 gangliosidosis with ataxia that were treated with ADLL in individual-cases of off-label-use gait significantly improved, supporting the concept that ADLL and ALL may also be efficacious in multiple LSDs and other neurodegenerative diseases.

In conclusion, we have found that a well-tolerated drug, ADLL, and its enantiomer ALL slow disease progression and improve motor function and lipid accumulation in murine and cell models of NPC1. Furthermore, in observational studies in NPC1 patients, treatment with ADLL was associated with improvement in multiple neurological domains and a significant reduction in the rate of disease progression, potentially via restoration of aerobic

metabolism based on the mechanistic studies conducted in the *Npc1*^{-/-} mouse model. The striking synergy of ADLL with miglustat in *Npc1*^{-/-} mice suggests that combining these two drugs will lead to improved short- and long-term clinical outcomes and merits clinical trials. It is interesting to note that 12 of the 13 NPC1 patients in the observational clinical study were on the standard of care miglustat, so part of their clinical improvement may be the result of the synergy between the two disease modifying drugs. The individual enantiomers ALL and ADL have not yet been tested in combination with miglustat. The finding that both a mouse model of Sandhoff disease and GM2 gangliosides patients, regardless of age of onset, also showed clinical improvement when treated with ADLL suggest that this, and related analogues, may have broader utility in LSDs and more common neurodegenerative diseases. Based on ALL being the neuroprotective enantiomer, clinical trials with ALL are currently being conducted (NPC (NCT03759639), GM2 gangliosidosis (NCT03759665) and Ataxia-Telangiectasia (NCT03759678)).

Acknowledgements

We thank Ines Debove, MD, Joan Michelis, MD and Susanne Schneider, MD, PhD for blinded scoring of the GM2 gangliosidosis patient videos.

Funding

FP is a Wellcome Investigator in Science and a Wolfson Royal Society Merit Award Holder. EK was supported by Niemann-Pick UK, NPSuisse and Horizon 2020 - Marie Skłodowska-Curie Research and Innovation Staff Exchange (RISE) (Lysomod) program. Additional funding was from Niemann-Pick Research Foundation. We thank Dr. Marlene Moser for supporting us with patient examinations. Some work for this study was done at Great Ormond Street Hospital and the UCL Great Ormond Street Institute of Child Health, which received funding from the UK Department of Health's NIHR Biomedical Research Centres funding scheme.

Competing Interest

FP is a cofounder, shareholder and consultant to IntraBio and consultant to Actelion. PF is a shareholder in IntraBio. TBE received honoraria for lecturing from Actelion and Sanofi-Genzyme. MS is Joint Chief Editor of the Journal of Neurology, Editor in Chief of Frontiers of Neuro-otology and Section Editor of F1000. He has received speaker's honoraria from Abbott, Actelion, Auris Medical, Biogen, Eisai, Grünenthal, GSK, Henning Pharma, Interacoustics, Merck, MSD, Otometrics, Pierre-Fabre, TEVA, UCB. He is a shareholder of IntraBio. He acts as a consultant for Abbott, Actelion, AurisMedical, Heel, IntraBio and Sensorion.

References

- Boland B, Smith DA, Mooney D, Jung SS, Walsh DM, Platt FM. Macroautophagy is not directly involved in the metabolism of amyloid precursor protein. *J Biol Chem* 2010; 285: 37415–37426.
- Bremova T, Malinova V, Amraoui Y, Mengel E, Reinke J, Kolnikova M, et al. Acetyl-DL-leucine in Niemann-Pick type C: A case series. *Neurology* 2015; 85: 1368–1375.
- Chida J, Yamane K, Takei T, Kido H. An efficient extraction method for quantitation of adenosine triphosphate in mammalian tissues and cells. *Anal Chim Acta* 2012; 727: 8–12.
- Churchill GC, Strupp M, Galione A, Platt FM. Unexpected differences in the pharmacokinetics of N-acetyl-DL-leucine enantiomers after oral dosing and their clinical relevance. *PLoS One* 2020; 15: e0229585.
- Colaco A, Kaya E, Adriaenssens E, Davis LC, Zampieri S, Fernández-Suárez ME, et al. Mechanistic convergence and shared therapeutic targets in Niemann-Pick disease type C and Tangier disease. *J Inher Metab Dis* 2019: 1–12.
- Cortina-Borja M, Te Vruchte D, Mengel E, Amraoui Y, Imrie J, Jones SA, et al. Annual severity increment score as a tool for stratifying patients with Niemann-Pick disease type C and for recruitment to clinical trials. *Orphanet J Rare Dis* 2018; 13: 1–16.
- Dahl NK, Reed KL, Daunais MA, Faust JR, Liscum L. Isolation and characterization of Chinese hamster ovary cells defective in the intracellular metabolism of low density lipoprotein-derived cholesterol. *J Biol Chem* 1992; 267: 4889–4896.
- Günther L, Beck R, Xiong G, Potschka H, Jahn K, Bartenstein P, et al. N-Acetyl-L-Leucine accelerates vestibular compensation after unilateral labyrinthectomy by action in the cerebellum and thalamus. *PLoS One* 2015; 10: 1–18.
- Harris A, Paxton R, Powell SM, Gillim SE. Physiological Covalent Regulation of Rat Liver Branched-Chain α -Ketoacid Dehydrogenase. *Arch Biochem Biophys* 1985; 243: 542–555.
- Harris R a, Joshi M, Jeung NH, Obayashi M. Overview of the molecular and biochemical basis of branched-chain amino acid catabolism. *J Nutr* 2005; 135: 1527S–30S.
- Higaki K, Ninomiya H, Sugimoto Y, Suzuki T, Taniguchi M, Niwa H, et al. Isolation of NPC1-deficient Chinese hamster ovary cell mutants by gene trap mutagenesis. *J Biochem* 2001; 129: 875–880.
- Highstein SM, Holstein GR. The Anatomy of the vestibular nuclei. *Prog Brain Res* 2005; 151: 157–203.
- Huiyun L, Walter WF. PGC-1 α : a key regulator of energy metabolism. *Adv Physiol Educ* 2006; 30: 145–151.
- Jeyakumar M, Butters TD, Cortina-Borja M, Hunnam V, Proia RL, Perry VH, et al. Delayed symptom onset and increased life expectancy in Sandhoff disease mice treated with N-butyldeoxynojirimycin. *Proc Natl Acad Sci U S A* 1999; 96: 6388–93.

Jha MK, Jeon S, Suk K. Pyruvate Dehydrogenase Kinases in the Nervous System: Their Principal Functions in Neuronal-glia Metabolic Interaction and Neuro-metabolic Disorders. *Curr Neuropharmacol* 2012; 10: 393–403.

Kato M, Wynn RM, Chuang JL, Tso SC, Machius M, Li J, et al. Structural Basis for Inactivation of the Human Pyruvate Dehydrogenase Complex by Phosphorylation: Role of Disordered Phosphorylation Loops. *Structure* 2008; 16: 1849–1859.

Kaya E, Smith DA, Smith C, Boland B, Strupp M, Platt FM. Beneficial Effects of Acetyl-DL-Leucine (ADLL) in a Mouse Model of Sandhoff Disease. [Internet]. *J Clin Med* 2020; 9 Available from: <http://www.ncbi.nlm.nih.gov/pubmed/32276303>

Kennedy BE, Hundert AS, Goguen D, Weaver ICG, Karten B. Presymptomatic Alterations in Amino Acid Metabolism and DNA Methylation in the Cerebellum of a Murine Model of Niemann-Pick Type C Disease. *Am J Pathol* 2016; 186: 1–18.

Kennedy BE, LeBlanc VG, Mailman TM, Fice D, Burton I, Karakach TK, et al. Pre-symptomatic activation of antioxidant responses and alterations in glucose and pyruvate metabolism in niemann-pick type C1-deficient murine brain. *PLoS One* 2013; 8: e82685.

Kimball SR, Shantz LM, Horetsky RL, Jefferson LS. Leucine regulates translation of specific mRNAs in L6 myoblasts through mTOR-mediated changes in availability of eIF4E and phosphorylation of ribosomal protein S6. *J Biol Chem* 1999; 17: 11647–52.

Kirkegaard T, Gray J, Priestman DA, Wallom KL, Atkins J, Olsen OD, et al. Heat shock protein-based therapy as a potential candidate for treating the sphingolipidoses. *Sci Transl Med* 2016; 8

Klionsky DJ, Emr SD. Autophagy as a regulated pathway of cellular degradation. *Science* (80-) 2000; 290: 1717–1721.

Liana Roberts Stein, Imai S. The dynamic regulation of NAD metabolism in mitochondria. *Trends Endocrinol Metab* 2012; 23: 420–428.

Lloyd-Evans E, Platt FM. Lipids on trial: The search for the offending metabolite in Niemann-Pick type C disease. *Traffic* 2010; 11: 419–428.

Morris MD, Bhuvaneshwaran C, Shio H, Fowler S. Lysosome lipid storage disorder in NCTR-BALB/c mice. I. Description of the disease and genetics. *Am J Pathol* 1982; 2: 140–149.

Murphy MP, Hartley RC. Mitochondria as a therapeutic target for common pathologies. *Nat Rev Drug Discov* 2018; 1: 865–886.

Nagamori S, Wiriyasermkul P, Okuda S, Kojima N, Hari Y, Kiyonaka S, et al. Structure-activity relations of leucine derivatives reveal critical moieties for cellular uptake and activation of mTORC1-mediated signaling. *Amino Acids* 2016; 48: 1045–1058.

Pankiv S, Clausen TH, Lamark T, Brech A, Bruun JA, Outzen H, et al. p62/SQSTM1 binds directly to Atg8/LC3 to facilitate degradation of ubiquitinated protein aggregates by autophagy. *J Biol Chem* 2007; 282: 24131–45.

Patterson MC, Vecchio D, Prady H, Abel L, Wraith JE. Miglustat for treatment of Niemann-

Pick C disease: a randomised controlled study. *Lancet Neurol* 2007; 6: 765–772.

Paulina Ordonez M, Roberts EA, Kidwell CU, Yuan SH, Plaisted WC, Goldstein LSB, et al. Disruption and therapeutic rescue of autophagy in a human neuronal model of Niemann pick type C1. *Hum Mol Genet* 2012; 21: 2651–2662.

Pentchev PG, Gal AE, Booth AD, Omodeo-Sale F, Fours J, Neumeyer BA, et al. A lysosomal storage disorder in mice characterized by a dual deficiency of sphingomyelinase and glucocerebrosidase. *Biochim Biophys Acta - Lipids Lipid Metab* 1980; 3: 669–79.

Platt FM, Boland B, van der Spoel AC. The cell biology of disease: lysosomal storage disorders: the cellular impact of lysosomal dysfunction. *J Cell Biol* 2012; 199: 723–34.

Pliss L, Hausknecht KA, Stachowiak MK, Dlugos CA, Richards JB, Patel MS. Cerebral Developmental Abnormalities in a Mouse with Systemic Pyruvate Dehydrogenase Deficiency. *PLoS One* 2013; 8: 1–14.

Priestman DA, Van Der Spoel AC, Butters TD, Dwek RA, Platt FM. N-butyldeoxynojirimycin causes weight loss as a result of appetite suppression in lean and obese mice. *Diabetes, Obes Metab* 2008; 2: 159–66.

Ruiz-Rodado V, Nicoli ER, Probert F, Smith DA, Morris L, Wassif CA, et al. 1H NMR-Linked Metabolomics Analysis of Liver from a Mouse Model of NP-C1 Disease. *J Proteome Res* 2016; 15: 3511–3527.

Sango K, Yamanaka S, Hoffmann A, Okuda Y, Grinberg A, Westphal H, et al. Mouse models of Tay–Sachs and Sandhoff diseases differ in neurologic phenotype and ganglioside metabolism. *Nat Genet* 1995; 2: 170–6.

Schniepp R, Strupp M, Wuehr M, Jahn K, Dieterich M, Brandt T, et al. Acetyl-DL-leucine improves gait variability in patients with cerebellar ataxia—a case series. *Cerebellum & ataxias* 2016; 3: 8.

Son SM, Park SJ, Lee H, Siddiqi F, Lee JE, Menzies FM, et al. Leucine Signals to mTORC1 via Its Metabolite Acetyl-Coenzyme A. *Cell Metab* 2018; 0: 1–10.

Srivastava S. Emerging therapeutic roles for NAD(+) metabolism in mitochondrial and age-related disorders. *Clin Transl Med* 2016; 5: 25.

Strupp M, Teufel J, Habs M, Feuerecker R, Muth C, Van De Warrenburg BP, et al. Effects of acetyl-dl-leucine in patients with cerebellar ataxia: A case series. *J Neurol* 2013; 260: 2556–2561.

Tighilet B, Leonard J, Bernard-Demanze L, Lacour M. Comparative analysis of pharmacological treatments with N-acetyl-dl-leucine (Tanganil) and its two isomers (N-acetyl-L-leucine and N-acetyl-D-leucine) on vestibular compensation: Behavioral investigation in the cat. *Eur J Pharmacol* 2015; 769: 342–349.

Da Veiga Moreira J, Peres S, Steyaert JM, Bigan E, Paulevé L, Nogueira ML, et al. Cell cycle progression is regulated by intertwined redox oscillators. *Theor Biol Med Model* 2015; 12: 1–14.

Vibert N, Vidal P-P. *In vitro* effects of acetyl- dl -leucine (tanganil®) on central vestibular neurons and vestibulo-ocular networks of the guinea-pig. *Eur J Neurosci* 2001; 13: 735–748.

Te Vruchte D, Speak AO, Wallom KL, Al Eisa N, Smith DA, Hendriksz CJ, et al. Relative acidic compartment volume as a lysosomal storage disorder-associated biomarker. *J Clin Invest* 2014; 124: 1320–1328.

Williams IM, Wallom K, Smith DA, Eisa N Al, Smith C, Platt FM. Neurobiology of Disease Improved neuroprotection using miglustat , curcumin and ibuprofen as a triple combination therapy in Niemann – Pick disease type C1 mice. *Neurobiol Dis* 2014; 67: 9–17.

Xie C, Burns DK, Turley SD, Dietschy JM. Cholesterol is sequestered in the brains of mice with Niemann-Pick Type C disease but turnover is increased. *J Neuropathol Exp Neurol* 2000; 59: 1106–1117.

Yanagisawa H, Ishii T, Endo K, Kawakami E, Nagao K, Miyashita T, et al. L-leucine and SPNS1 coordinately ameliorate dysfunction of autophagy in mouse and human Niemann-Pick type C disease. *Sci Rep* 2017; 7: 1–9.

Yanjanin NM, Vélez JI, Gropman A, King K, Bianconi SE, Conley SK, et al. Linear clinical progression, independent of age of onset, in Niemann-Pick disease, type C. *Am J Med Genet Part B Neuropsychiatr Genet* 2010; 153B: 132–140.

Yudkoff M. Brain metabolism of branched-chain amino acids. *Glia* 1997; 21: 92–8.

Figure Legends

Figure 1. Acetyl leucine analogues impact on behavioural parameters in NPC1 mice.

For wild type untreated (*Npc1*^{+/+} UT), NPC1 untreated (*Npc1*^{-/-} UT), ADLL (*Npc1*^{-/-} ADLL), ALL (*Npc1*^{-/-} ALL), ADL (*Npc1*^{-/-} ADL) treatments min 5 animals, max 7 for each group. **p* < 0.05, ***p* < 0.01, ****p* < 0.001, *****p* < 0.0001. **A)** Symptomatic and pre-symptomatic AL treatment Y coordinates displacement of each consecutive foot from a straight-line trajectory. (Mean ± SD, n=6) **B)** Late stage AL treatment SEMs of Y coordinate changes (Mean ± SD, n=6; One-way ANOVA) **C)** Early stage AL treatment SEMs of Y coordinate changes (Mean ± SD, n=6; One-way ANOVA). **D)** Early stage AL treatment front and hind duty cycle measurements, mean ± SD, (2-way ANOVA) **E)** Early stage AL treatments front and hind stand mean measurements, min 5 animals per group, Mean ± SD, (2-way ANOVA). Duty Cycle and Stand mean analyses were measured by 3-recorded runs per animal and quantitative results were obtained with Noldus CatWalk 10.5 software system. **F)** Early stage AL treatment motor performance measurements, min 5 animals each group, Mean ± SD, (One-way ANOVA). Motor function performance was measured with accelerating Rotarod (1 rpm per minute up to 10 rpm). **G)** Life expectancy percentages and median survivals (Gehan-Breslow-Wilcoxon test) n=6.

Figure 2. Effect of Acetyl leucine analogues on biochemical and histopathology in *Npc1*^{-/-} mice at 59 days of age.

For all AL treatments n= 5 animals per group, for miglustat (positive control) (*Npc1*^{-/-} MIG) n= 2 or n= 1. **p* < 0.05, ***p* < 0.01, ****p* < 0.001, *****p* < 0.0001. **A)** Glycosphingolipid (GSL) profiles in brain, mean ± SD, (2-way ANOVA). **B)** Sphingosine levels in brain. Mean ± SD, (One-way ANOVA). **C)** Sphinganine levels in brain, mean ± SD, (One-way ANOVA). **D)** GSLs in cerebellum, mean ± SD, (2-way ANOVA). **E)** Sphingosine in cerebellum, mean ± SD, (One-way ANOVA). **F)** Sphinganine

in cerebellum, mean \pm SD, (One-way ANOVA). **G**) Cerebellum stained with calbindin-b (Purkinje cells, red) or CD68 (activated microglia, yellow). Scale bar 800 μ m. **H**) Purkinje cell density (Purkinje cell number normalised by perimeter of each lobule) at 59 days of age relative to NPC1 untreated, mean \pm SD, (2-way ANOVA) **I**) CD68 cell density (number of CD68 positive microglia per area) at 59 days of age, mean \pm SD, (One-way ANOVA).

Figure 3. Effect of Acetyl leucine analogues on non-neuronal tissues and cells. For all AL treatments n= 5 animals per group, for miglustat (positive control) (*Npc1*^{-/-} MIG) n= 2 or n= 1. **p*< 0.05, ***p*< 0.01, ****p*< 0.001, *****p*< 0.0001. **A**) GSLs in liver, mean \pm SD (2-way ANOVA). **B**) Sphingosine in liver, mean \pm SD, (One-way ANOVA) **C**) Sphinganine in liver, mean \pm SD, (One-way ANOVA). **D**) Liver cholesterol mean \pm SD, (One-way ANOVA). **E**) MitoSOX(red) and MitoTracker(Green) and LysoTracker(Green) changes relative to *Npc1*^{+/+} with 24 and 72h 1mM ALs. CHO cells were double stained with either MitoTracker Green and MitoSOX red, or LysoTracker Green and propidium iodide. Single and live cell populations and FITC and PE fluorescence were determined by analytical Flow Cytometry. Mean \pm SD, (2-way ANOVA). **F**) Sphingosine, total GSL and free cholesterol levels (72h) relative to *Npc1*^{+/+}, Mean \pm SD, (2-way ANOVA). **G**) NPC1 CHO cells stained with filipin (cyan, cholesterol) and propidium iodide (magenta, nucleus). Scale bar 20 micron.

Figure 4. Effect of ADLL in combination with miglustat. For wild type untreated (*Npc1*^{+/+} UT), NPC1 untreated (*Npc1*^{-/-} UT), ADLL (*Npc1*^{-/-} ADLL), miglustat (*Npc1*^{-/-} MIG) and combination (*Npc1*^{-/-} miglustat & ADLL) therapies min 5 animals for each group. **p*< 0.05, ***p*< 0.01, ****p*< 0.001, *****p*< 0.0001. **A**) Survival curves (percentage of life expectancy) and median survivals (Gehan-Breslow-Wilcoxon test). **B**) Body weight curves of experimental groups over the course of their life, mean \pm SD. **C**) Motor performance

measurements (Rotarod) at 8, 10 and 12 weeks of age, mean \pm SD (2-way ANOVA). Animals that did not perform the task were excluded from the experiment. **D)** Representative image of footprints of miglustat and miglustat/ADLL combination therapy relative to wild type **E)** Duty cycle measurements of front and hind paws at 10 weeks of age, Mean \pm SD, (2-way ANOVA) **F)** Stand mean measurements at of front and hind paws 10 weeks of age, Mean \pm SD, (2-way ANOVA).

Figure 5. Effects of acetyl leucine analogues on expression of proteins involved in nutrient sensing, autophagy, BCAA catabolism, and glutamate metabolism in cerebellum at 59 days of age. Wild type untreated (*Npc1*^{+/+} UT), NPC1 untreated (*Npc1*^{-/-} UT), ADLL (*Npc1*^{-/-} ADLL), ALL (*Npc1*^{-/-} ALL), ADL (*Npc1*^{-/-} ADL) treatments, n=5 for each group. **p* < 0.05, ***p* < 0.01, ****p* < 0.001, *****p* < 0.0001. **A)** mTOR, Phospho-mTOR expression and phospho-mTOR and mTOR ratio, Mean \pm SD (2-way ANOVA). **B)** LC3-I, LC3-II expression, LC3-II and LC3-I ratios, Mean \pm SD (2-way ANOVA). **C)** p62 levels, Mean \pm SD, (One-way ANOVA). **D)** Western blots images of phospho-mTOR, mTOR, LC3 and p62 and their beta-actin loading controls. **E)** BCKDH-A, pBCKDH-A, p/t BCKDH-A expression, mean \pm SD, (2-way ANOVA). **F)** BCKDHA, pBCKDHA, and GDH western blot images with beta-actin loading controls. **G)** GDH expression, mean \pm SD (One-way ANOVA).

Figure 6. Effects of acetyl leucine analogues on expression of proteins involved in energy metabolism and the antioxidant system in cerebellum at 59 days of age. Wild type untreated (*Npc1*^{+/+} UT), NPC1 untreated (*Npc1*^{-/-} UT), ADLL (*Npc1*^{-/-} ADLL), ALL (*Npc1*^{-/-} ALL), ADL (*Npc1*^{-/-} ADL) treatments, n=5 for each group. **p* < 0.05, ***p* < 0.01, ****p* < 0.001, *****p* < 0.0001. **A)** NAD, NADH, total NAD (NADt) measurements, mean \pm SD, (2-

way ANOVA). **B)** NADH/NADH ratios, mean \pm SD, (One-way ANOVA). **C)** ADP/ATP ratios mean \pm SD (One-way ANOVA). **D)** Western blot images of PDHC, pPDH, LDH, PGC-1alpha and beta-actin loading controls. **E)** PDHC protein expressions, Mean \pm SD, (2-way ANOVA). **F)** pPDH expressions and pPDH/PDHE1 alpha ratios, Mean \pm SD, (2-way ANOVA). **G)** LDH expression, Mean \pm SD, (One-way ANOVA). **H)** PDHE1 alpha/LDH ratios, Mean \pm SD, (One-way ANOVA). **I)** PGC 1 alpha expression, mean \pm SD (One-way ANOVA). **J)** PDK 1-2-4 and PDP1 expression, Mean \pm SD (2-way ANOVA). **K)** Western blot images of PDKs and PDP1 along with their beta-actin loading controls. **L)** SOD1 and SOD2 expression, mean \pm SD (2-way ANOVA). **M)** Western blot images of SOD1 and SOD2 along with beta-actin loading controls.

Figure 7. Clinical data from 13 adult NPC1 patients. For demographics see materials and methods **A)** Total clinical severity scores (maximum score 50, with higher values equating to increasing levels of disability (Yanjanin *et al.*, 2010)). Data were plotted prior to initiation of treatment with Tanganil™ (ADLL), incorporating available retrospective data **B)** Clinical data computed as Annual Severity Increment Scores (Cortina-Borja *et al.*, 2018), ($p < 0.001$ in ASIS score) **C)** Slope of total severity score (severity units per year) before and after ADLL treatment. Each individual participant in this observational study is colour coded.

Figure 8. Effects of Acetyl-DL-Leucine on behavioural and biochemical parameters in 12-week-old Sandhoff disease mice and GM2 patients. Sandhoff untreated (*Hexb*^{-/-} UT), ADLL (*Hexb*^{-/-}ADLL). 6-8 animals per group. **A)** Front-hind stand mean measurements of *Hexb*^{-/-} UT and *Hexb*^{-/-}ADLL, Mean \pm SD, * $p = 0.0323$, 2-way ANOVA. **B)** Front-hind step cycle measurements of *Hexb*^{-/-} UT and *Hexb*^{-/-}ADLL, Mean \pm SD, ** $p < 0.0063$, 2-way ANOVA. **C)** Percent improvement in clinical scores in three patients with GM2

gangliosidosis on baseline and after one month on medication with N-Acetyl-DL-Leucine (ADLL). Scale for Assessment and Rating of Ataxia (SARA) Montreal Cognitive Assessment (MoCA) and 8-M-Walking-Test (8 MWT) were assessed. 3rd patient was excluded from MoCA because the test is not approved for children. See also **Videos 1-2. D)** Unbiased Clinical Impression of Change in Severity (CI-CS) scores of GM2 patient videos. CI-CS Skala Clinical Impression of Change in Severity; 1=normal, not at all ill; 2=borderline ill; 3=mildly ill; 4=moderately ill; 5=markedly ill; 6=severely ill; 7=among the most extremely ill patients. Paired t test, $p=0.0039$. For individual scoring data see **Table 2**.

Figure 9. Summary table. Summary table of the effect of AL treatments on investigated pathologies *in vivo*, *ex vivo* and *in vitro*, along with the proposed mechanism of AL treatments in the cerebellum. Red arrows indicate the pathologies in NPC1 relative to its wild-type counterparts. Green arrows indicate the significant changes in response to acetyl-leucine treatment.

Table 1. Number of patients (total cohort $n=13$) that improved, stabilised or deteriorated following ADLL treatment stratified by the neurological domains scored (NIH NCSS).

Table 2. CI-CS scoring of 3 GM2 patients by 3 blinded and unbiased experts.

Video 1

A 28-year old male patient with juvenile-onset Tay-Sachs disease, Eight-Meter Walk Test is shown. Note the gait instability with increased fall risk at baseline. The patient is not able to walk independently, constant support of either assistant, or the wall is required. After one month on medication with N-Acetyl-DL-Leucine (ADLL), the patient has more postural

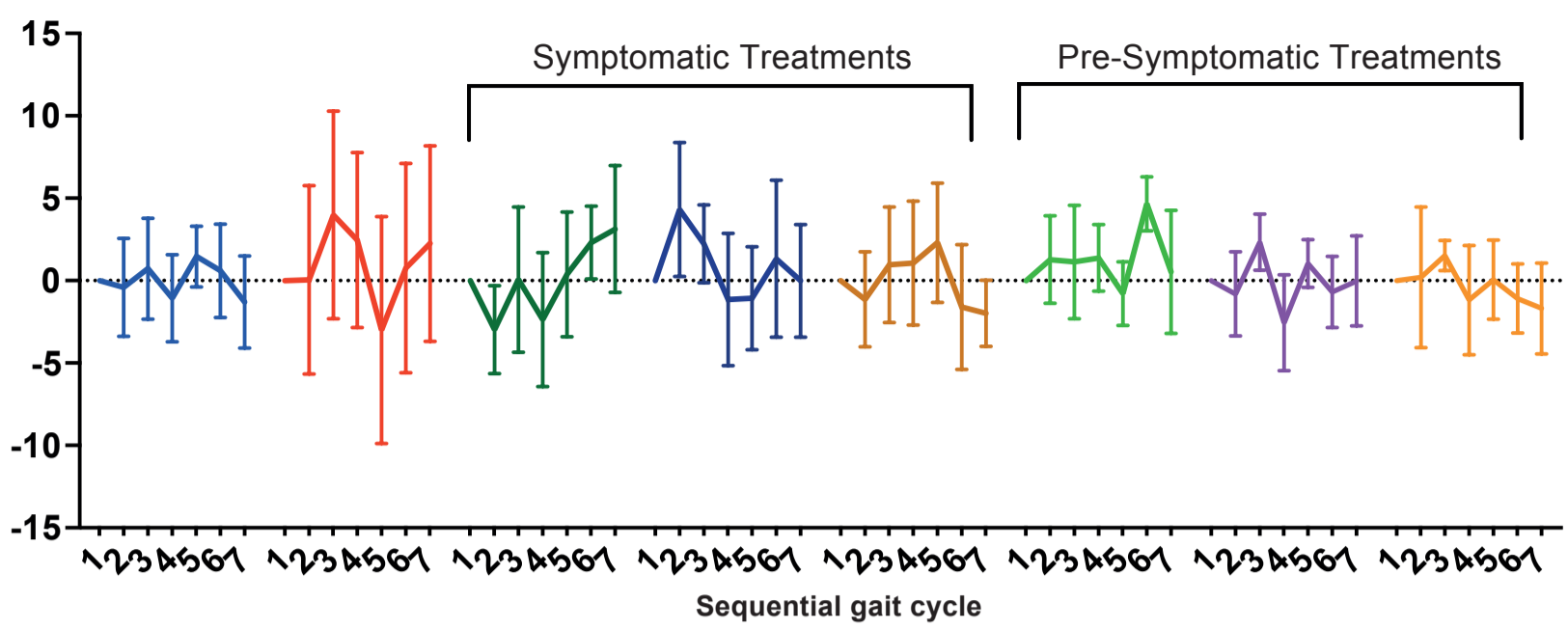
stability, the gait pattern changes with increased pace rate and reduced variability and postural sway.

Video 2

Eight-Meter-Walk-Test of a 32-year old female patient with adult-onset Tay-Sachs disease is shown prior to and after 1 month on medication with N-Acetyl-DL-Leucine (ADLL). Note the more stable nature of the gait pattern with decreased fall risk on medication.

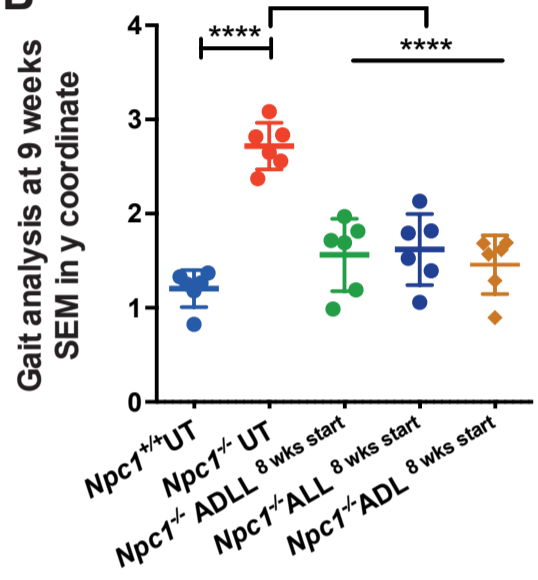
A
1
2
3
4
5
6
7
8
9
10
11
12
13
14
15
16
17
18
19
20
21
22
23
24
25
26
27
28
29
30
31
32
33
34
35
36
37
38
39
40
41
42
43
44
45
46
47
48
49
50
51
52
53
54
55
56
57
58
59
60

A
Gait analysis at 9 weeks
Changes in y coordinate

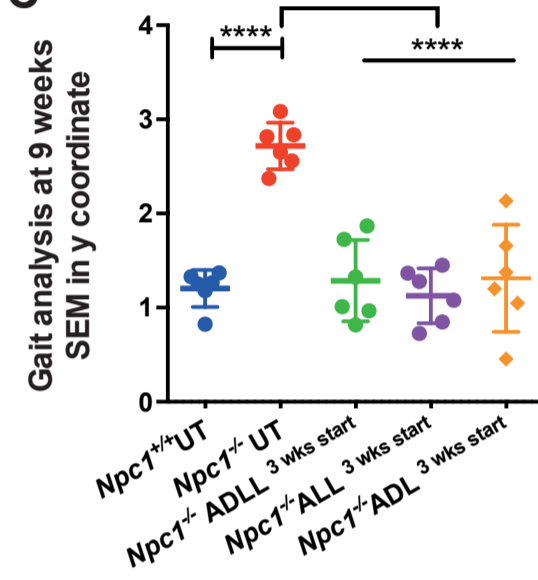


- *Npc1*^{+/+} UT
- *Npc1*^{-/-} UT
- *Npc1*^{-/-} ADLL 8 wks start
- *Npc1*^{-/-} ALL 8 wks start
- *Npc1*^{-/-} ADL 8 wks start
- *Npc1*^{-/-} ADLL 3 wks start
- *Npc1*^{-/-} ALL 3 wks start
- *Npc1*^{-/-} ADL 3 wks start

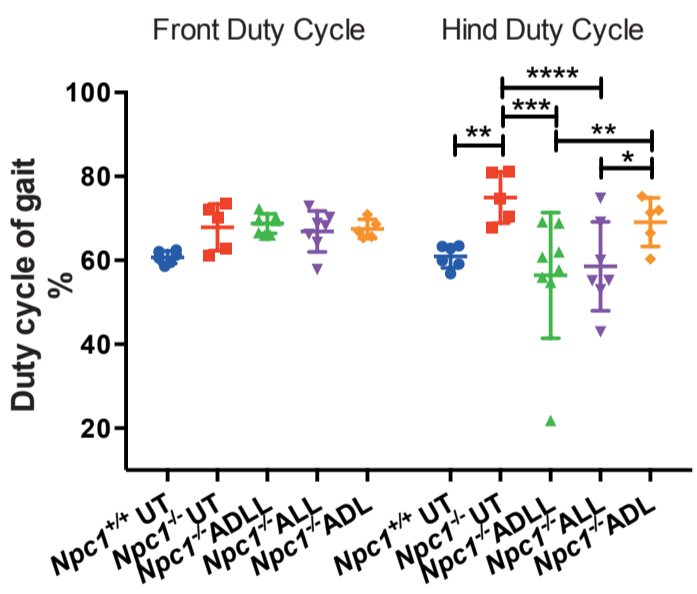
B



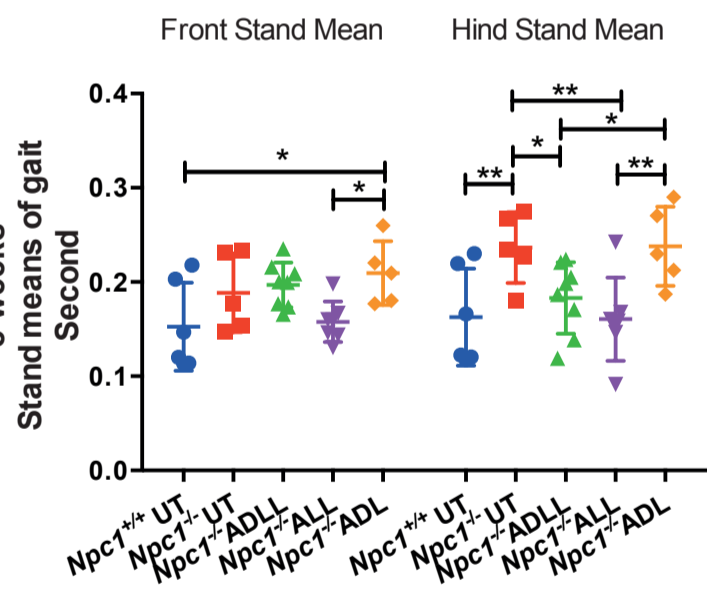
C



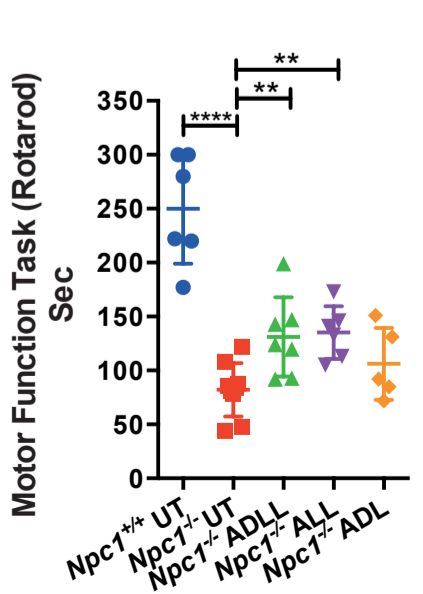
D



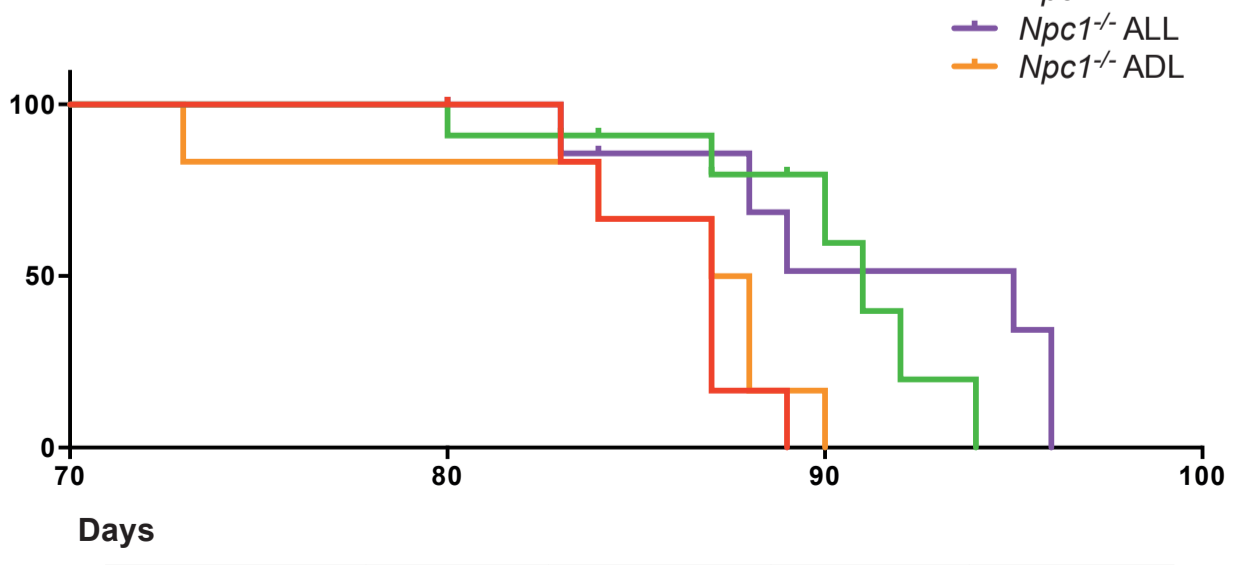
E



F

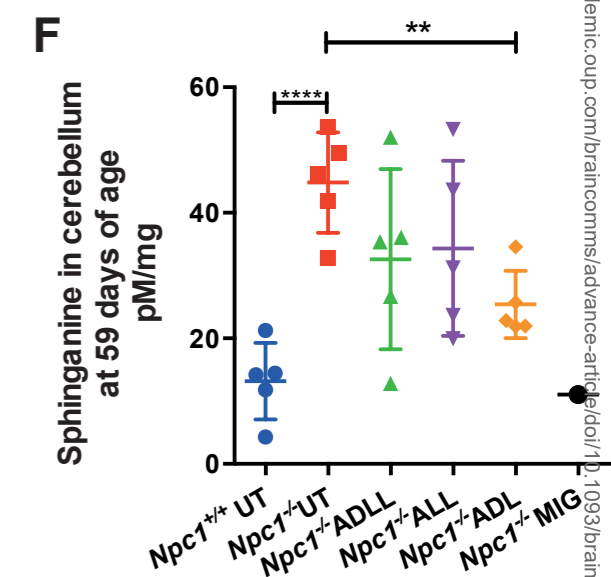
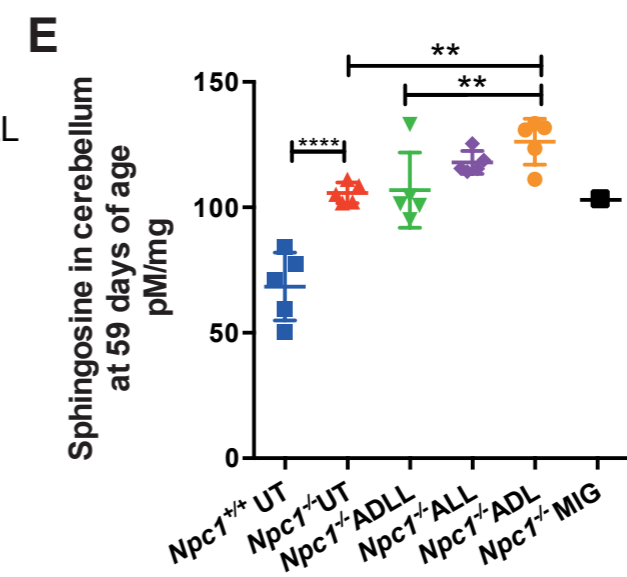
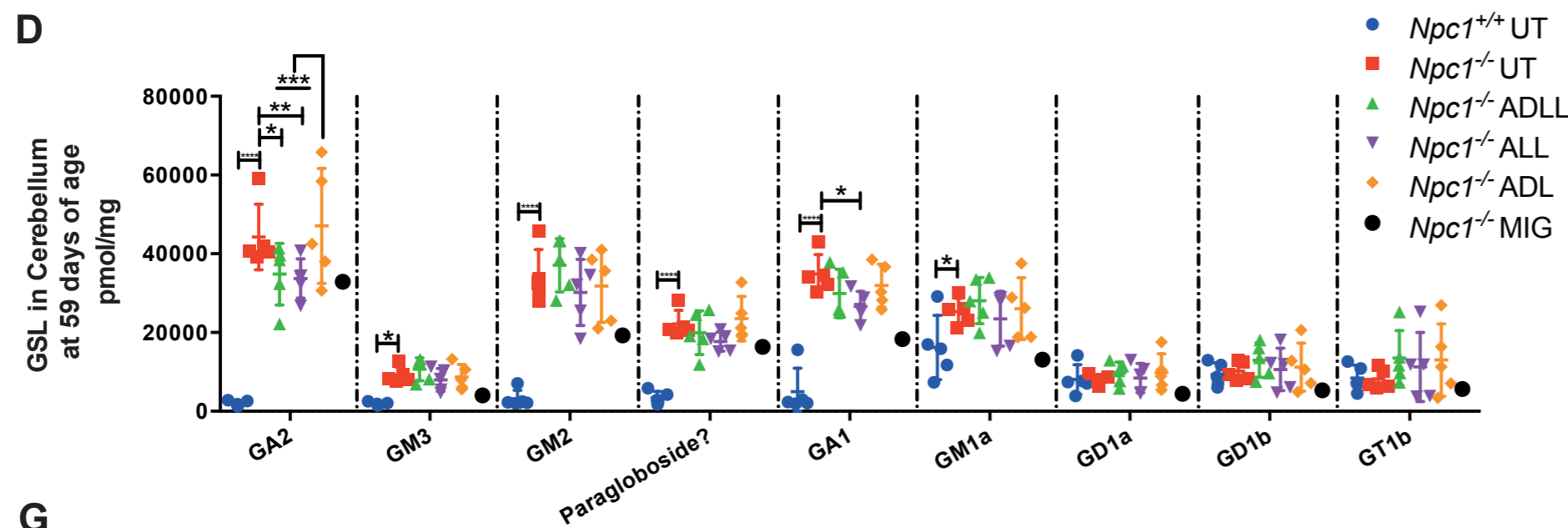
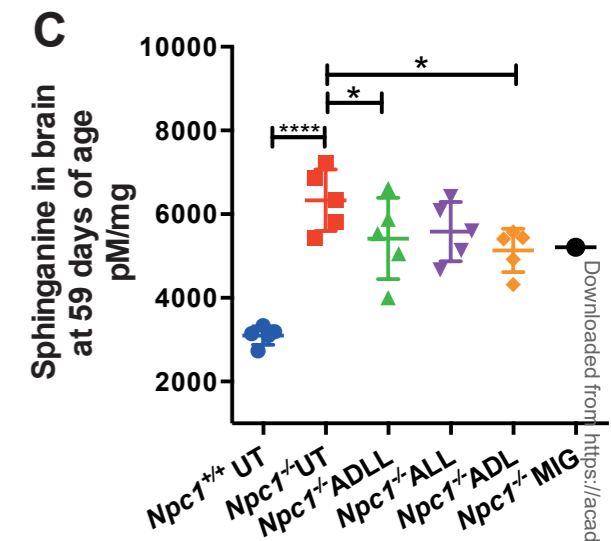
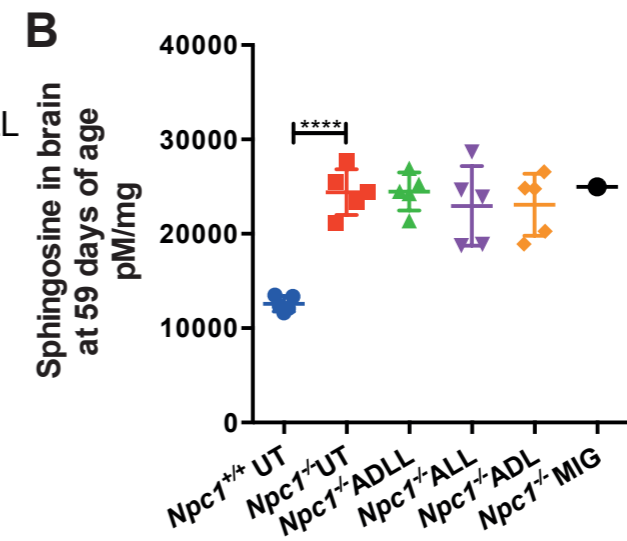
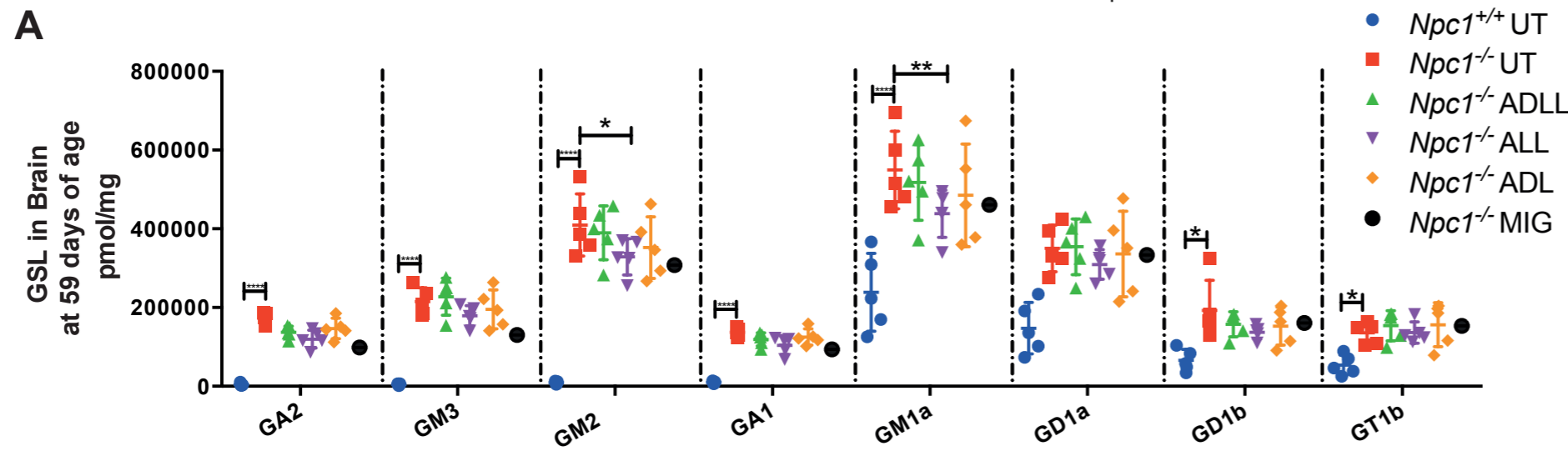


G

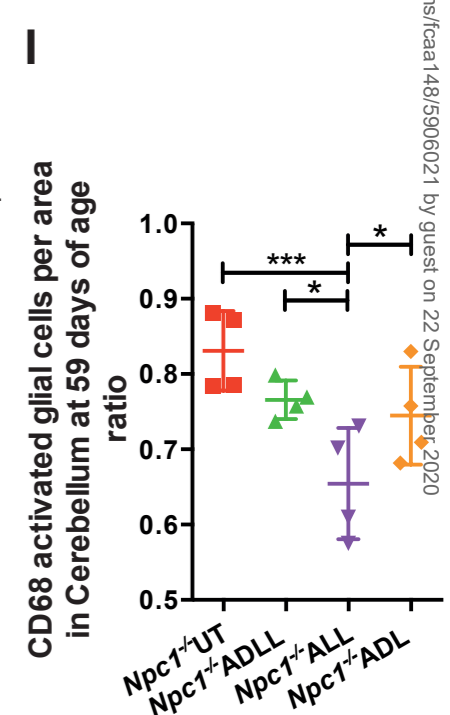
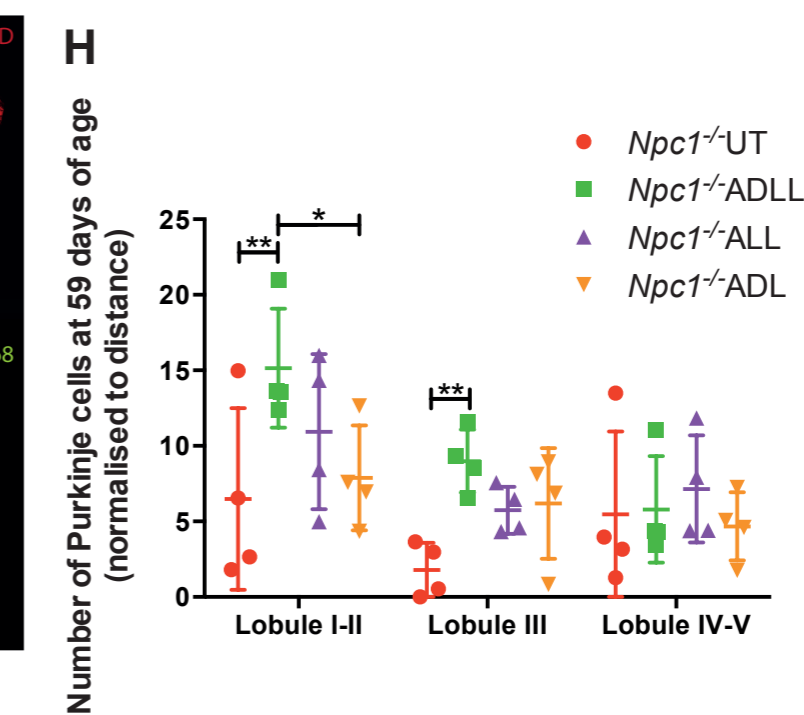
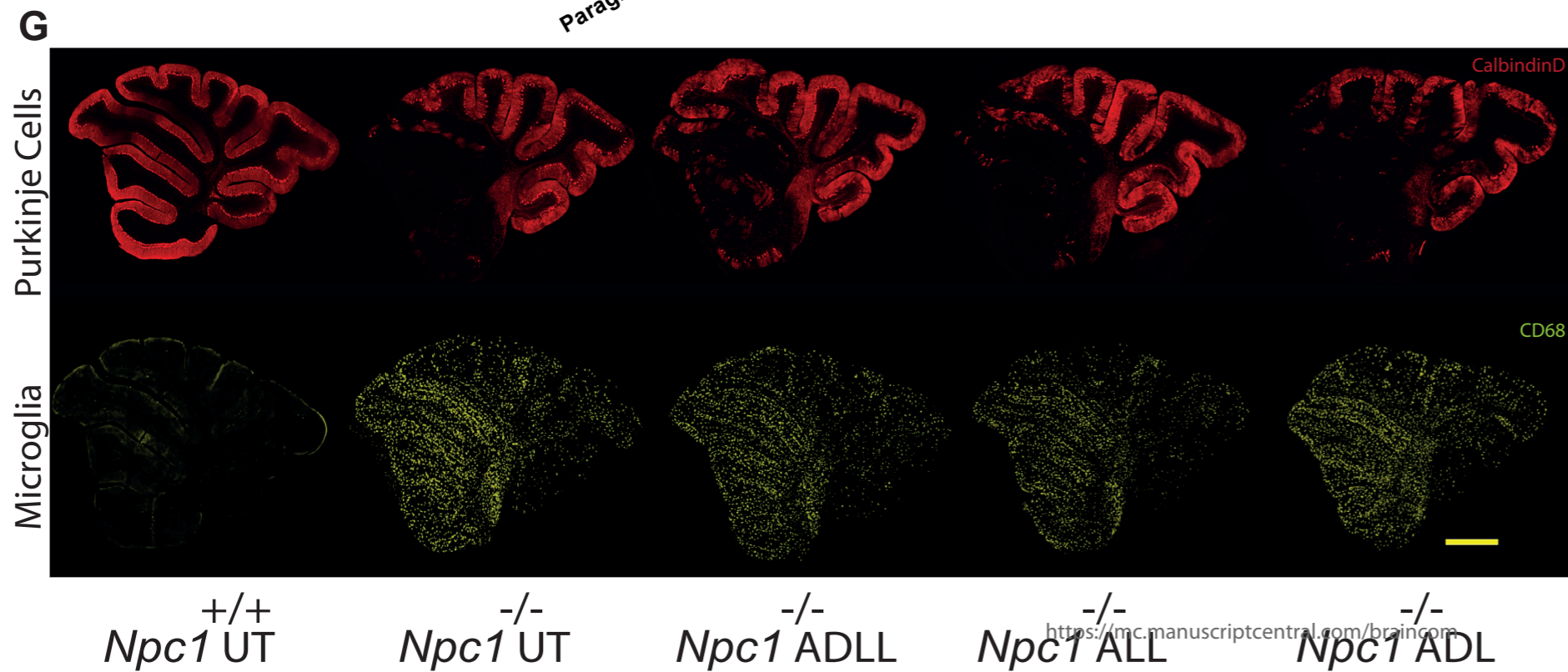


	<i>Npc1</i> ^{-/-} UT	<i>Npc1</i> ^{-/-} ADLL	<i>Npc1</i> ^{-/-} ALL	<i>Npc1</i> ^{-/-} ADL
Median survival (days)	87	91 (+4.5%)	95 (+9.1%)	87.5

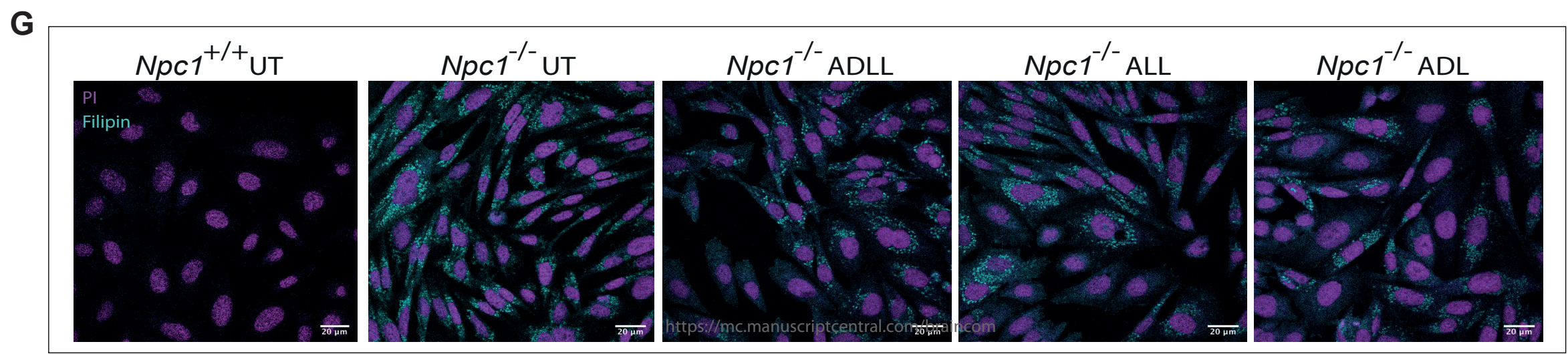
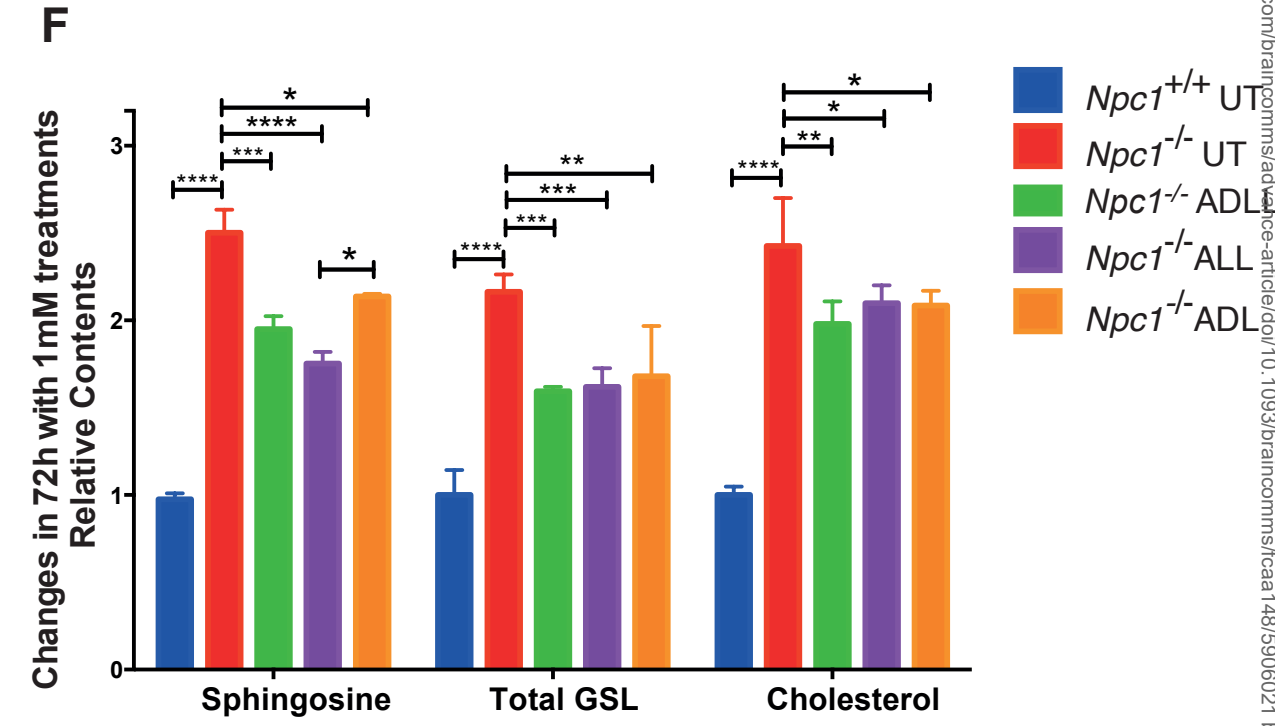
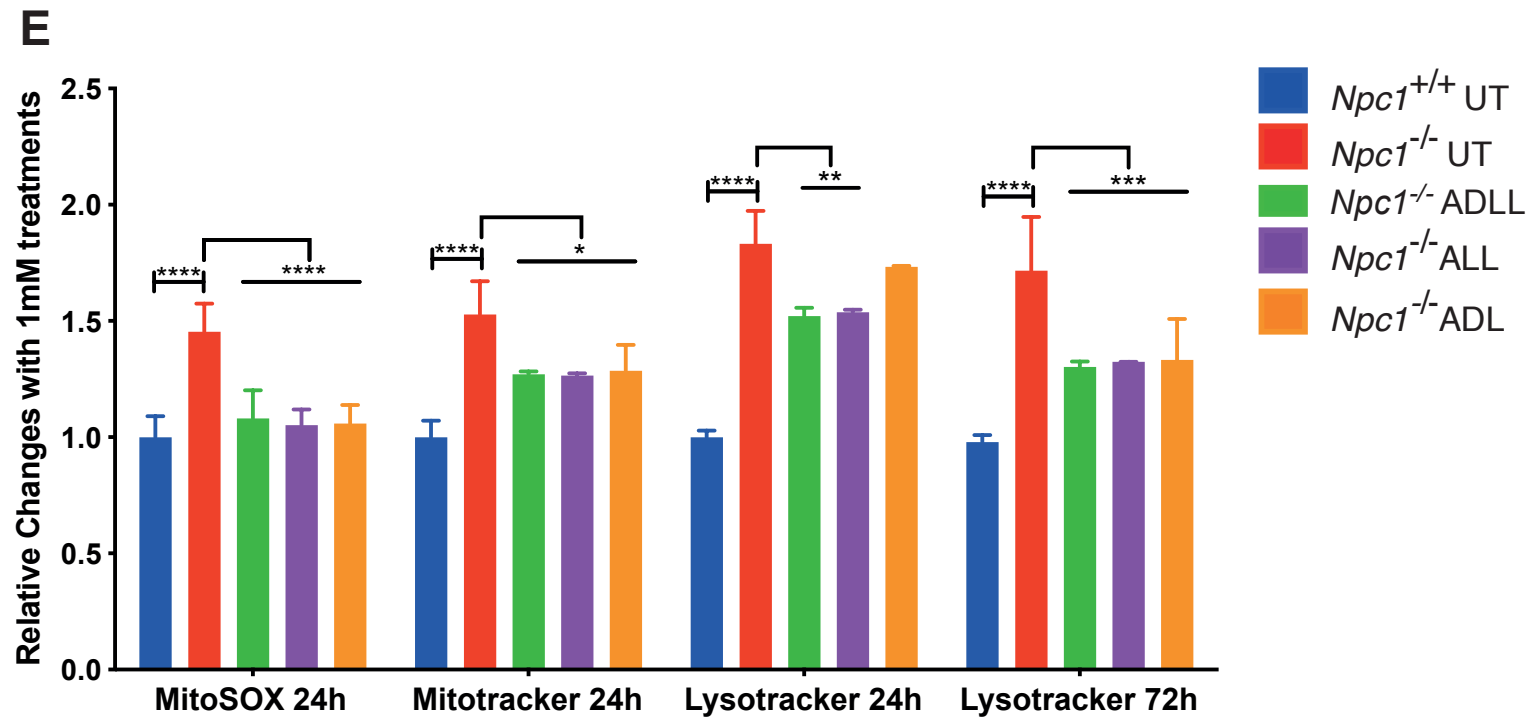
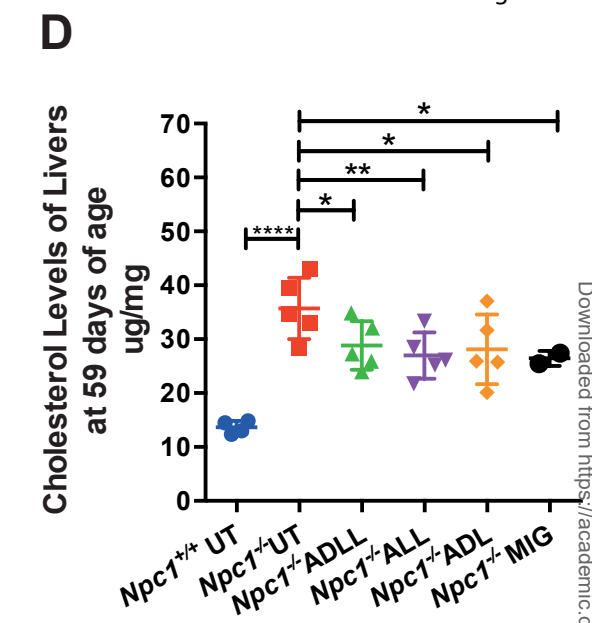
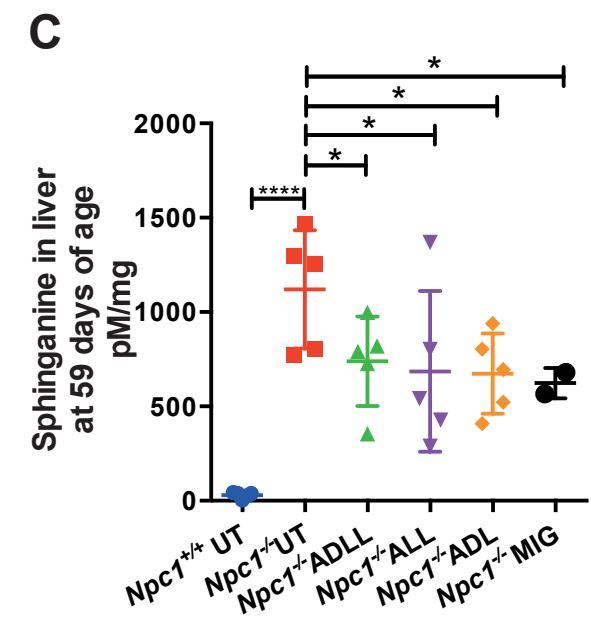
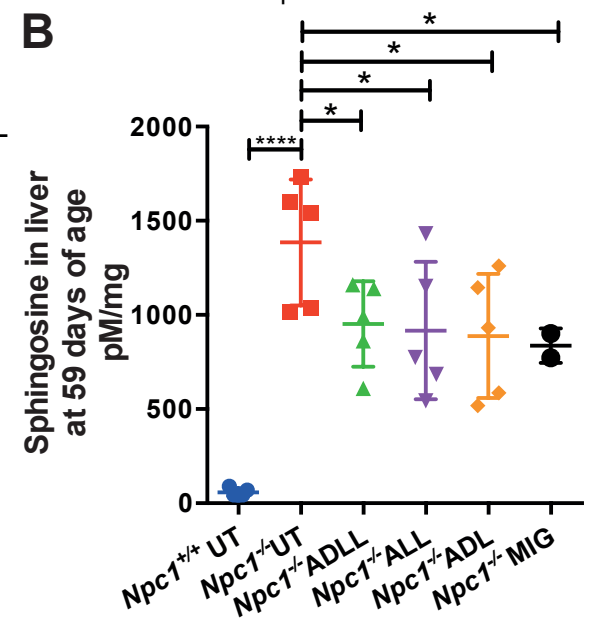
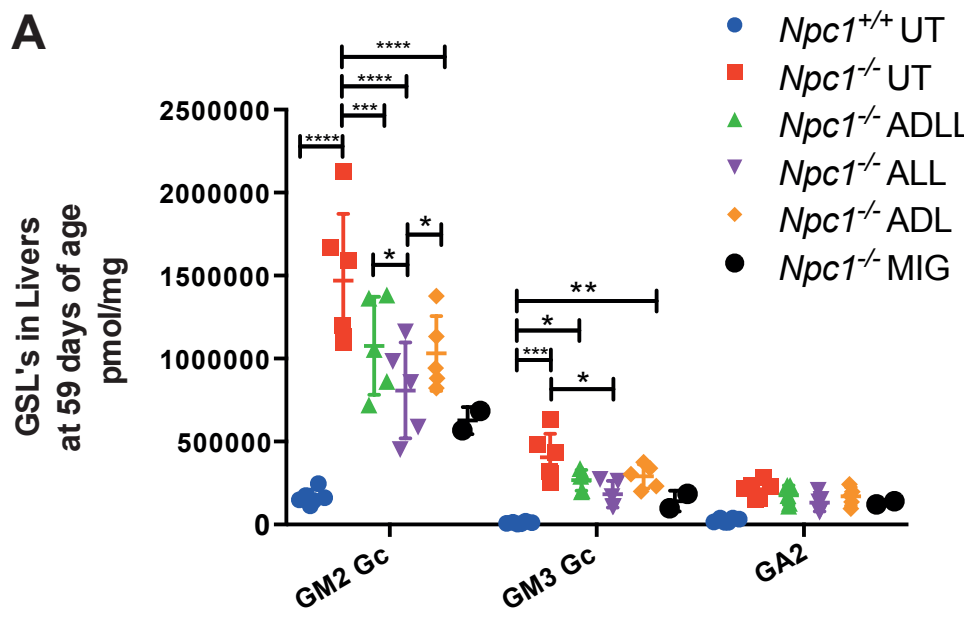
Brain

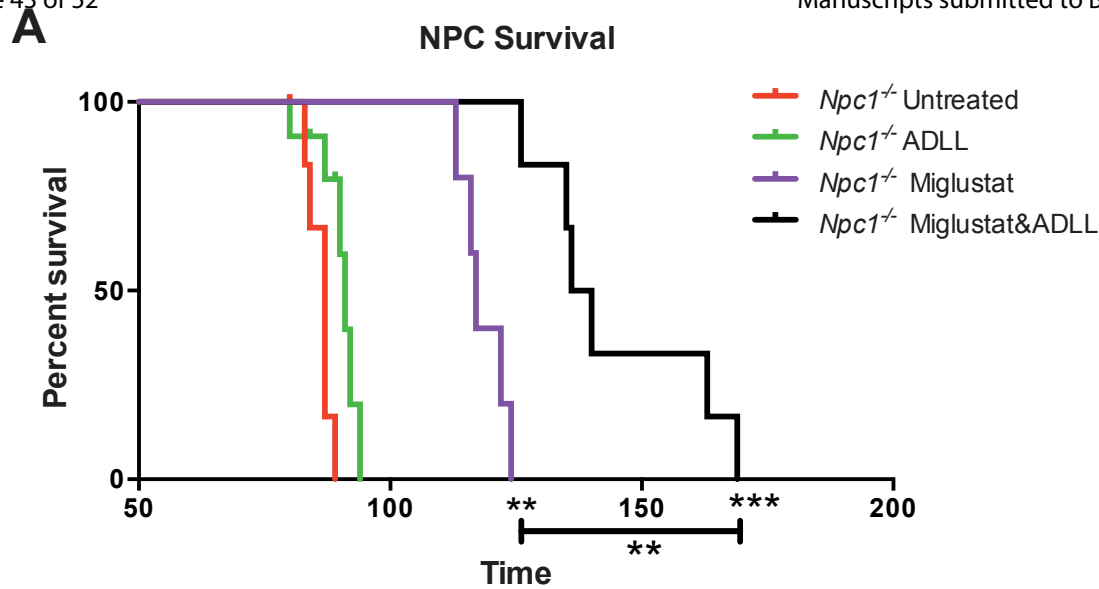


Cerebellum

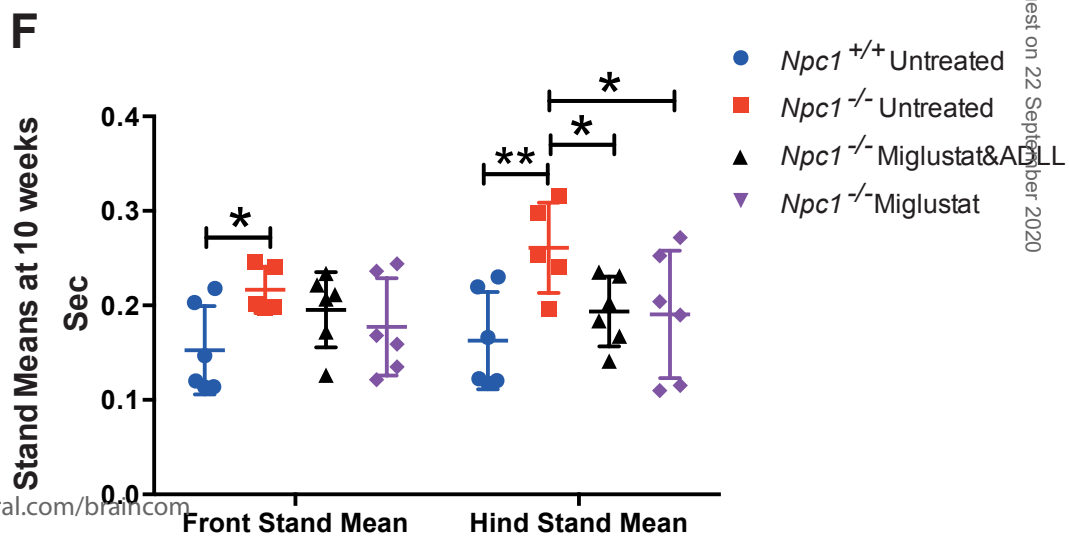
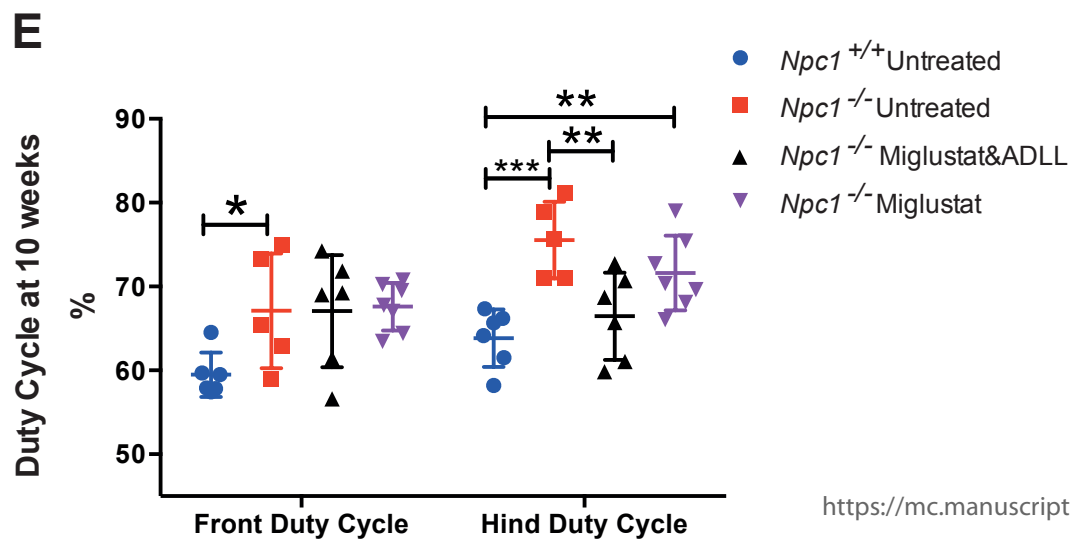
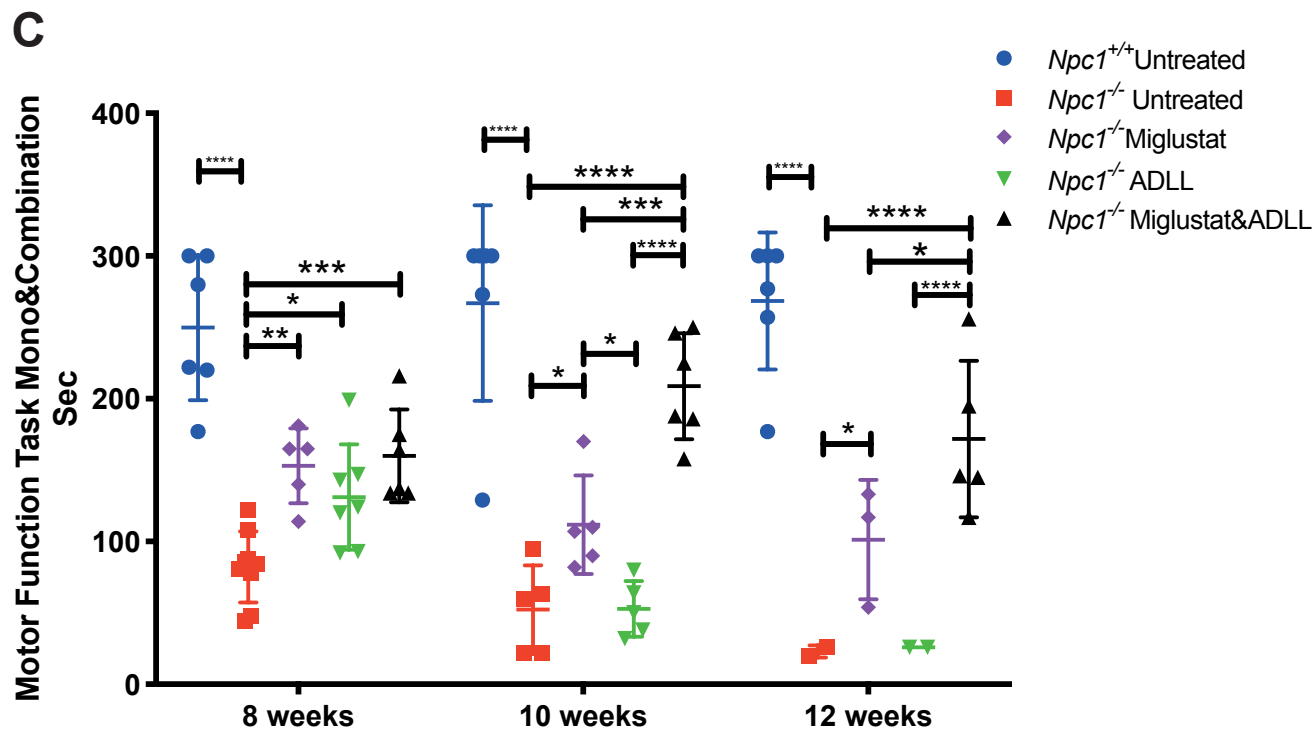
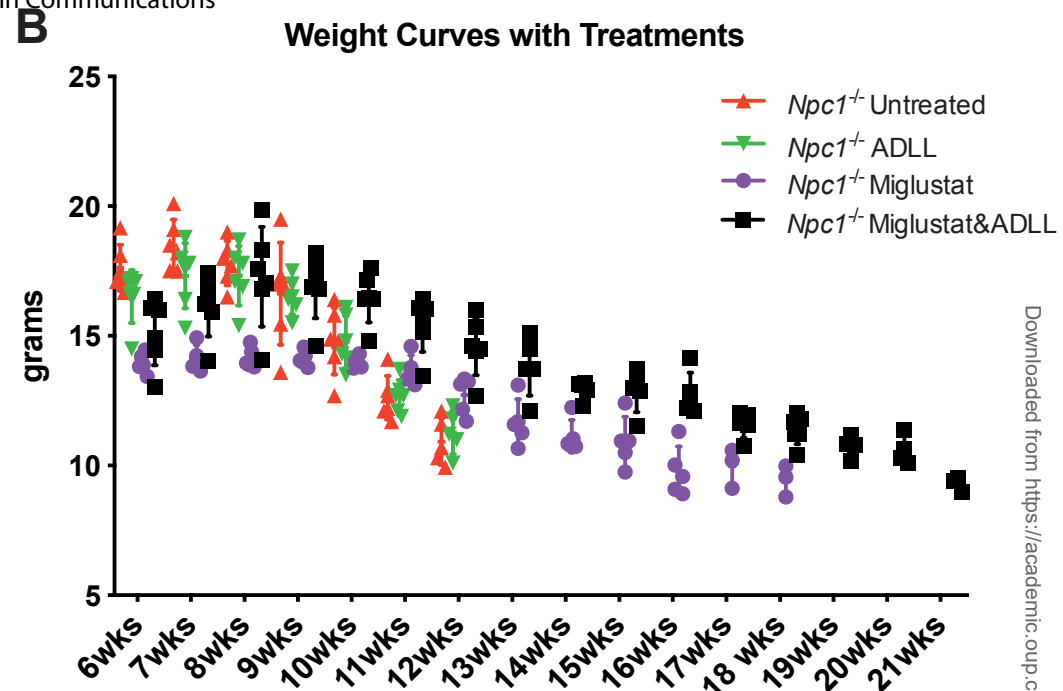


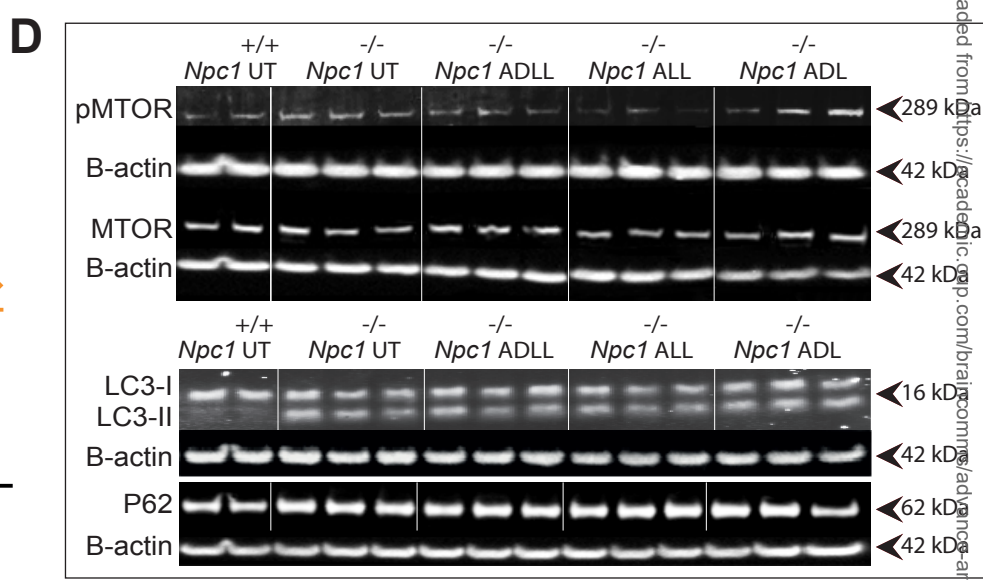
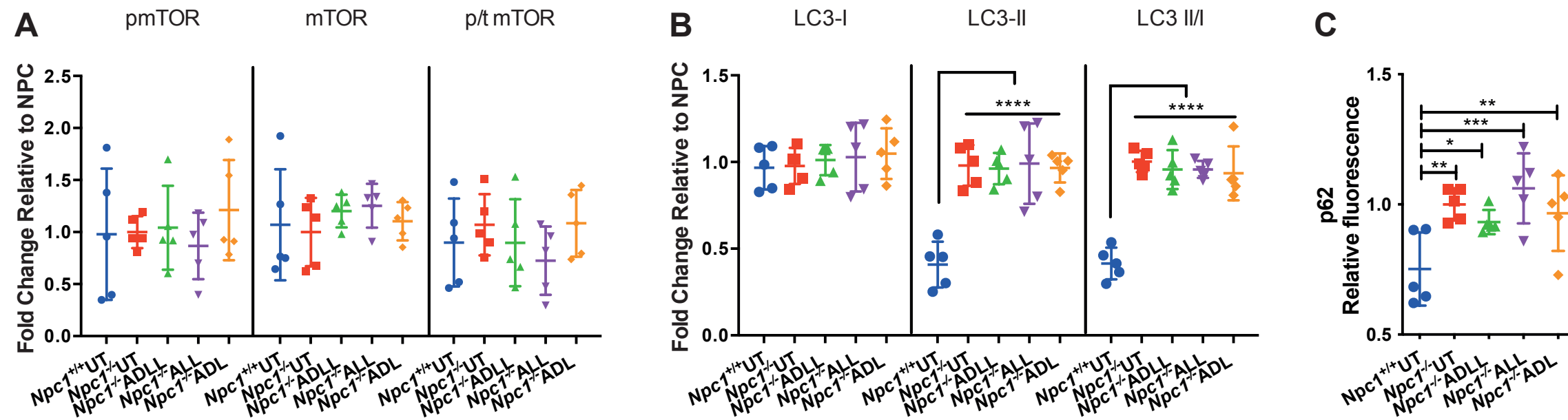
1
2
3
4
5
6
7
8
9
10
11
12
13
14
15
16
17
18
19
20
21
22
23
24
25
26
27
28
29
30
31
32
33
34
35
36
37
38
39
40
41
42
43
44
45
46
47
48
49
50
51
52
53
54
55
56
57
58
59
60



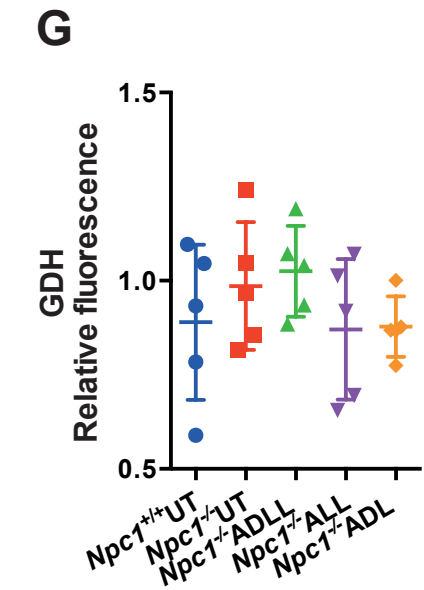
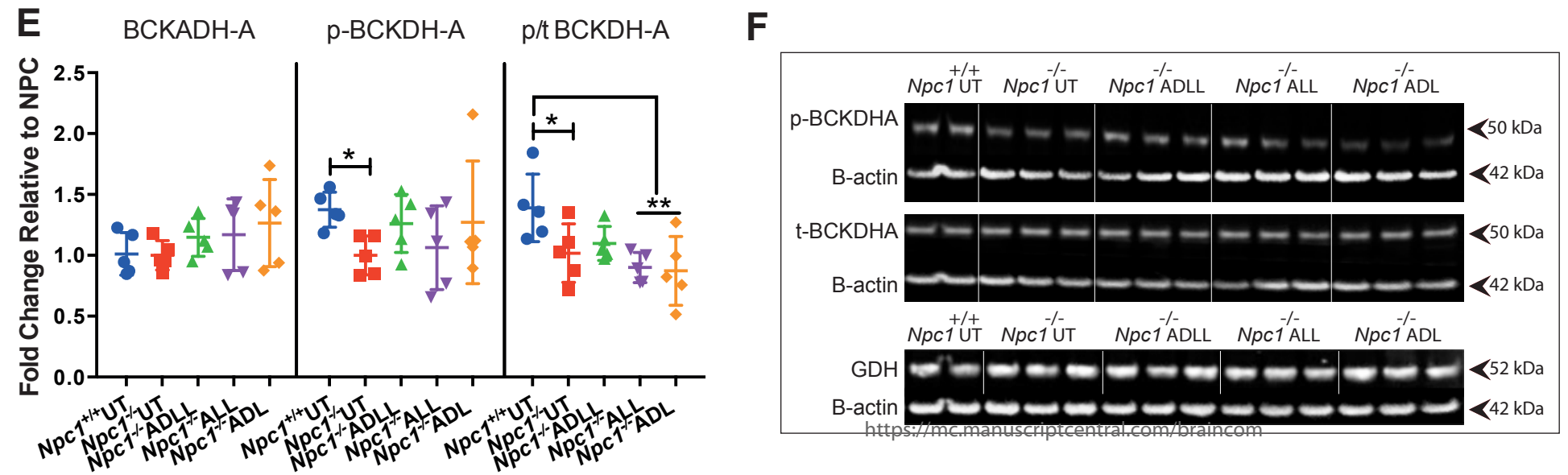


	$Npc1^{-/-}$ Miglustat	$Npc1^{-/-}$ Miglustat&ADLL	$Npc1^{-/-}$ Untreated	$Npc1^{-/-}$ ADLL
Median survival	117 (+34.4%)	138 (+58.6%)	87	91 (+4.5%)

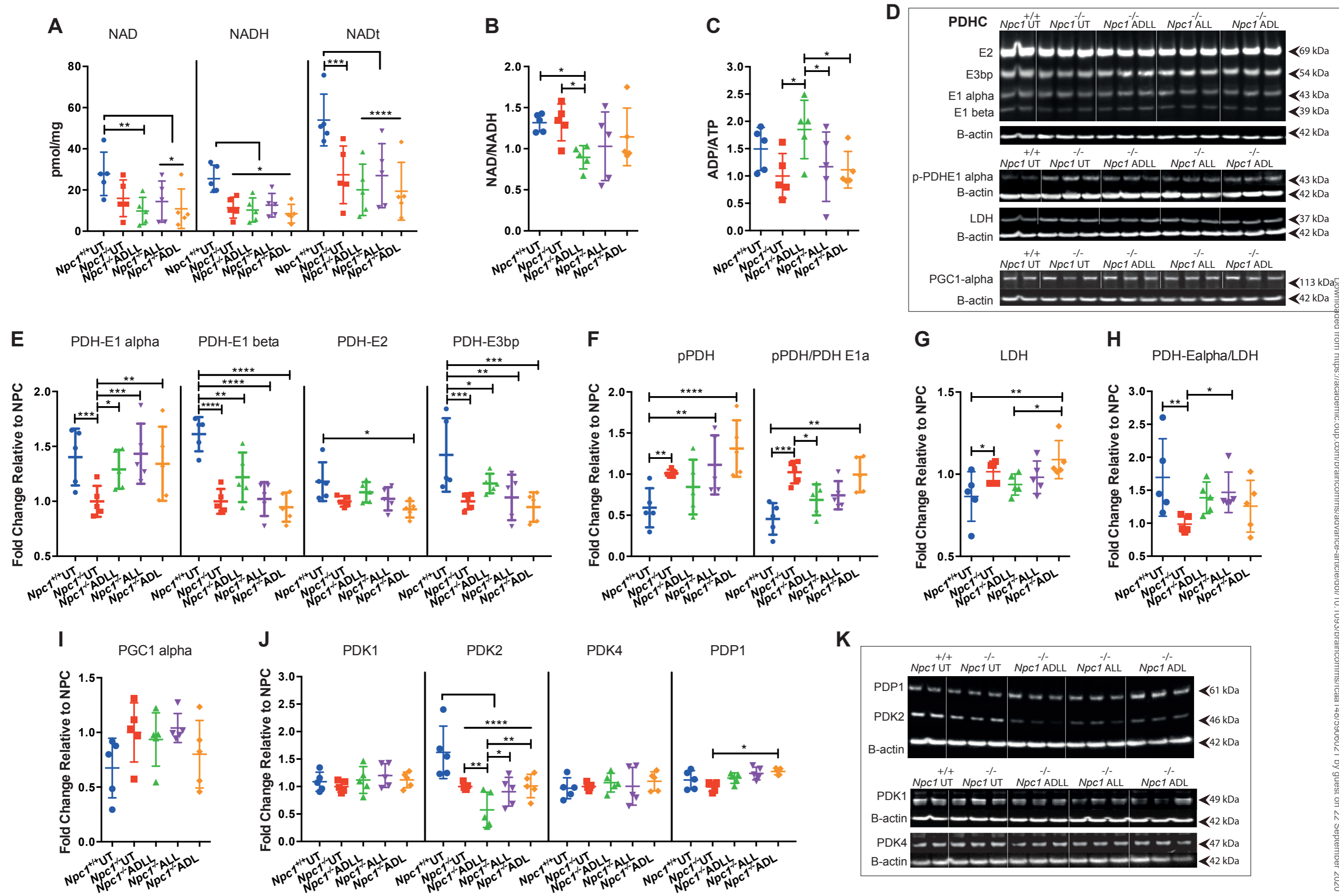




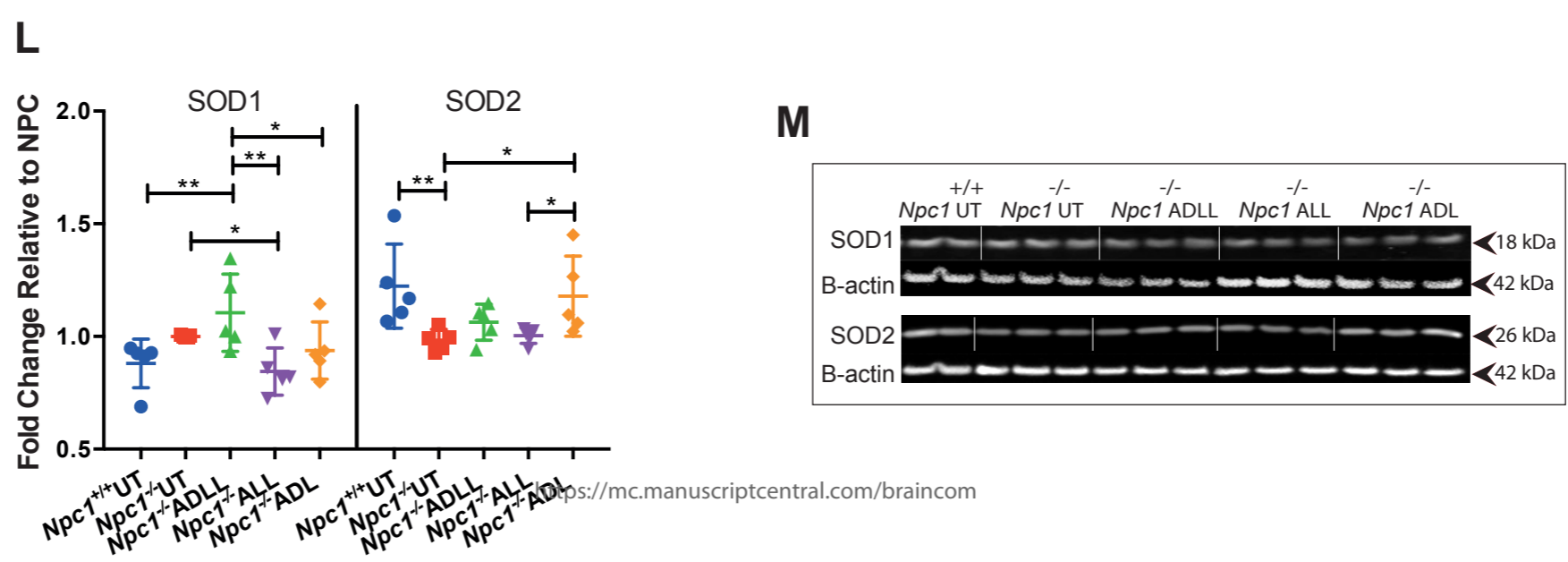
BCAA Catabolism/ Glutamate metabolism



Downloaded from https://academic.oup.com/braincomm/advance-article/doi/10.1093/braincomm/taaa148/5906021 by guest on 22 September 2020

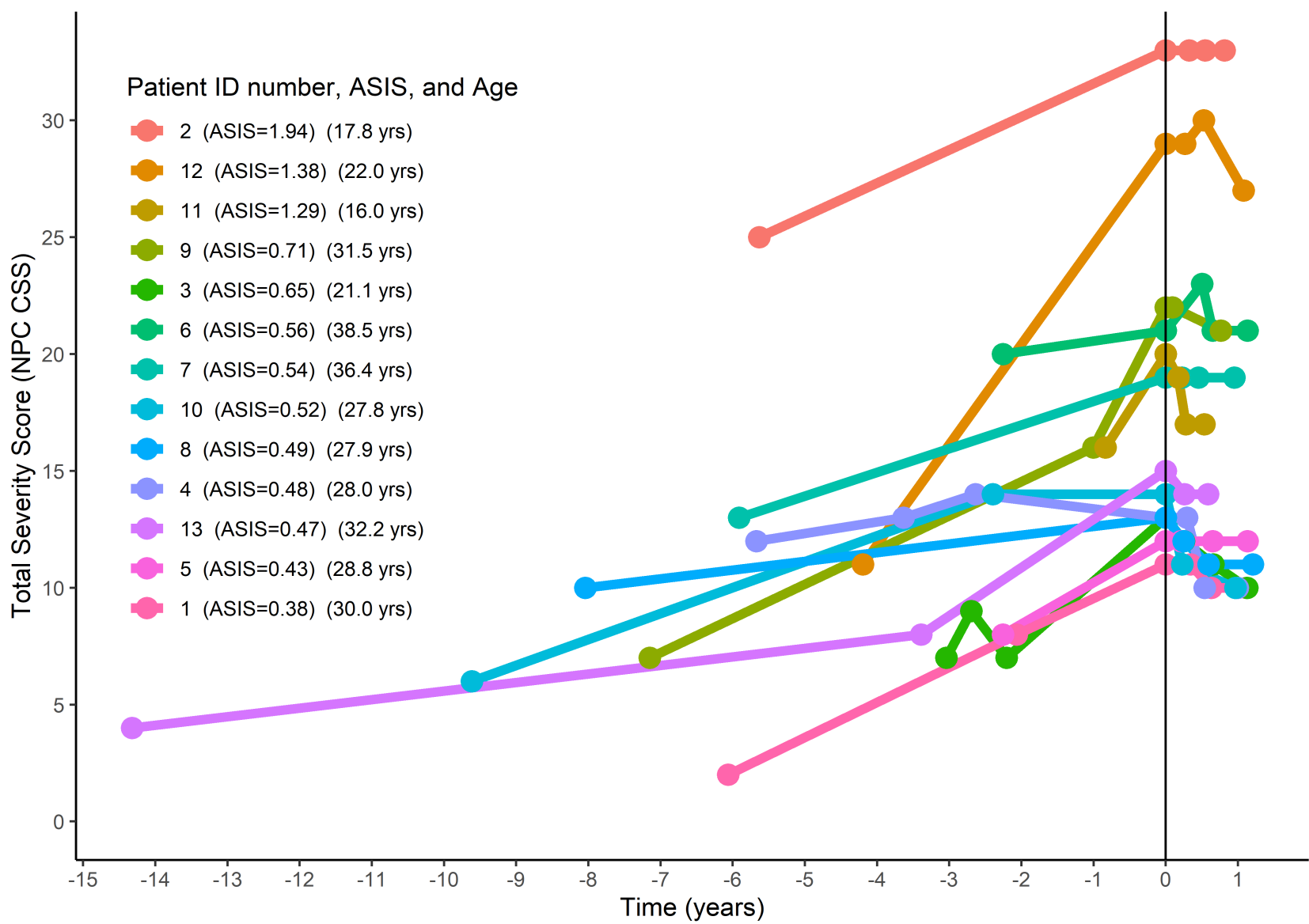


Antioxidant system

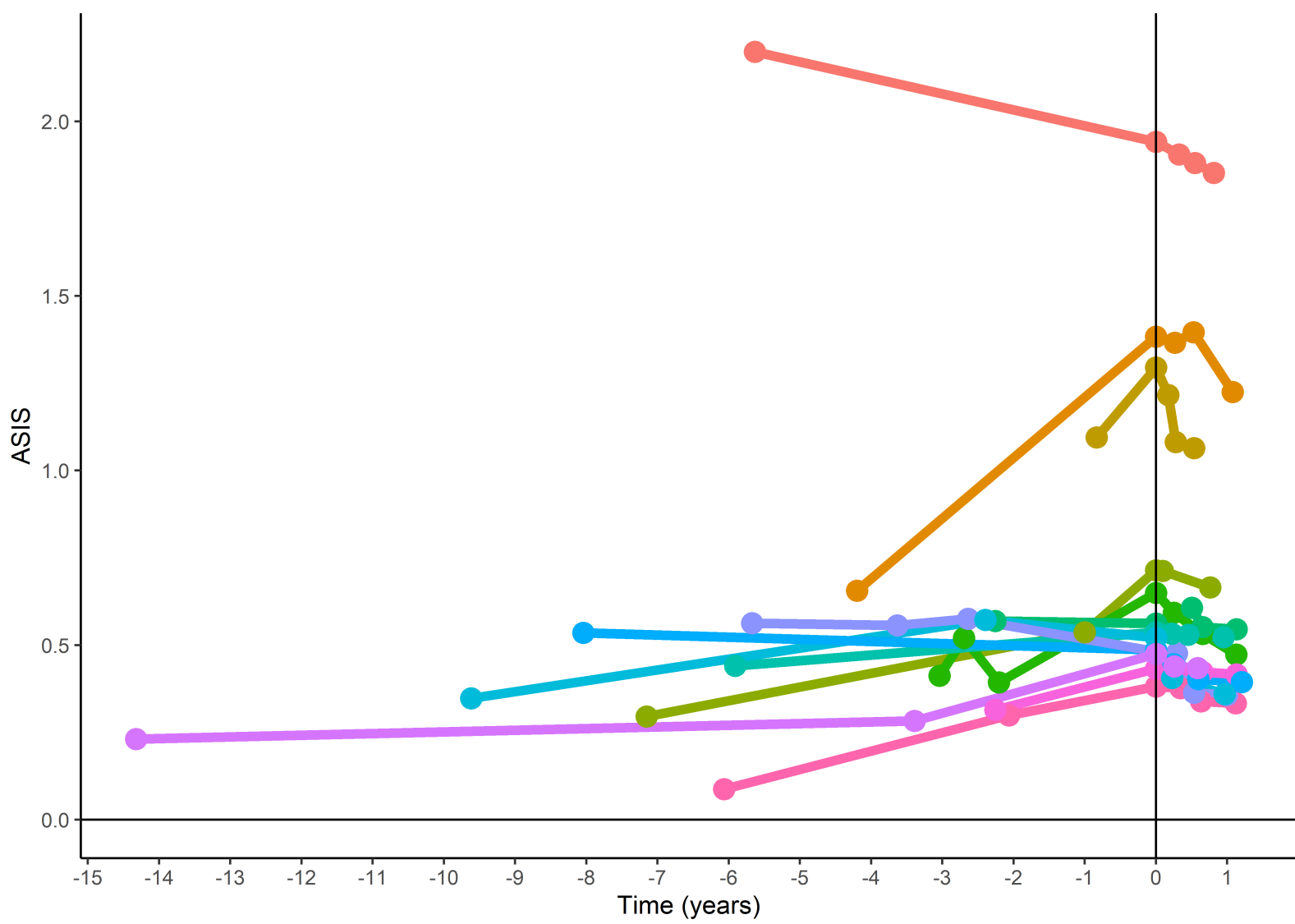


Downloaded from https://academic.oup.com/braincomms/advance-article/doi/10.1093/braincomms/aca148/5906021 by guest on 22 September 2020

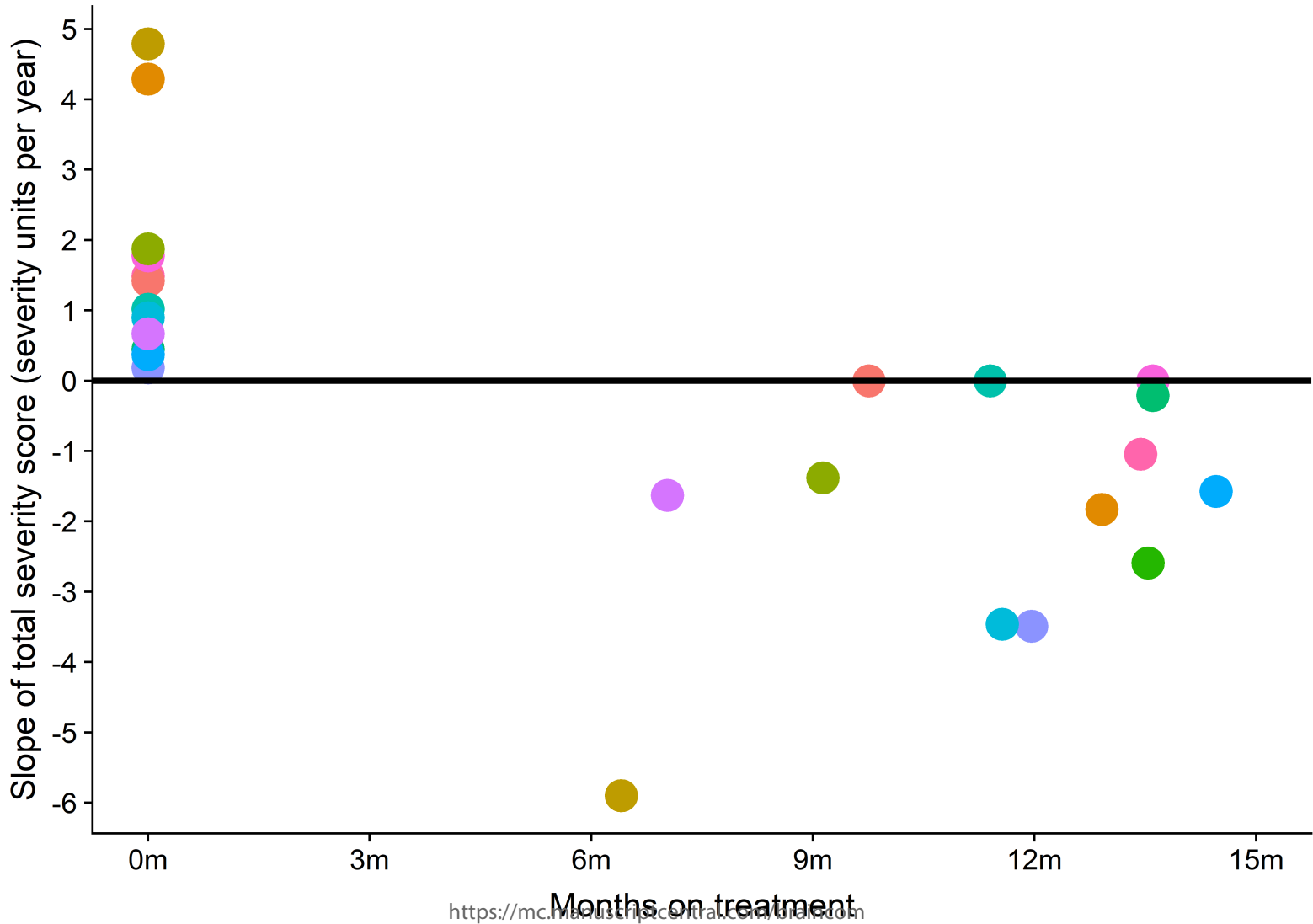
A



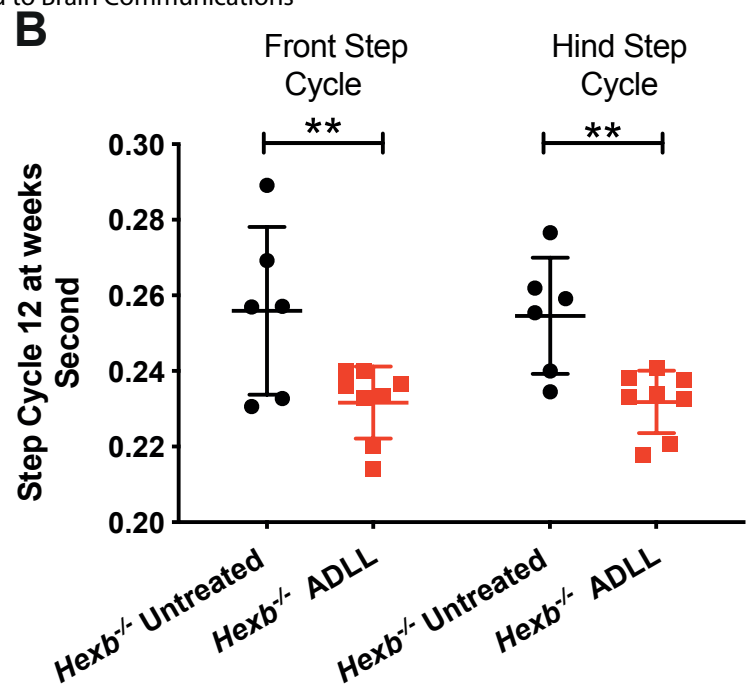
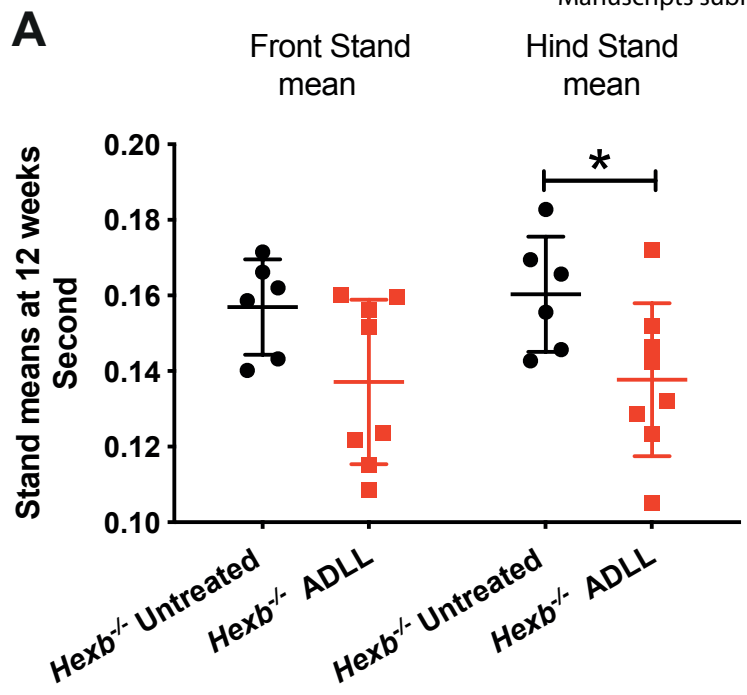
B



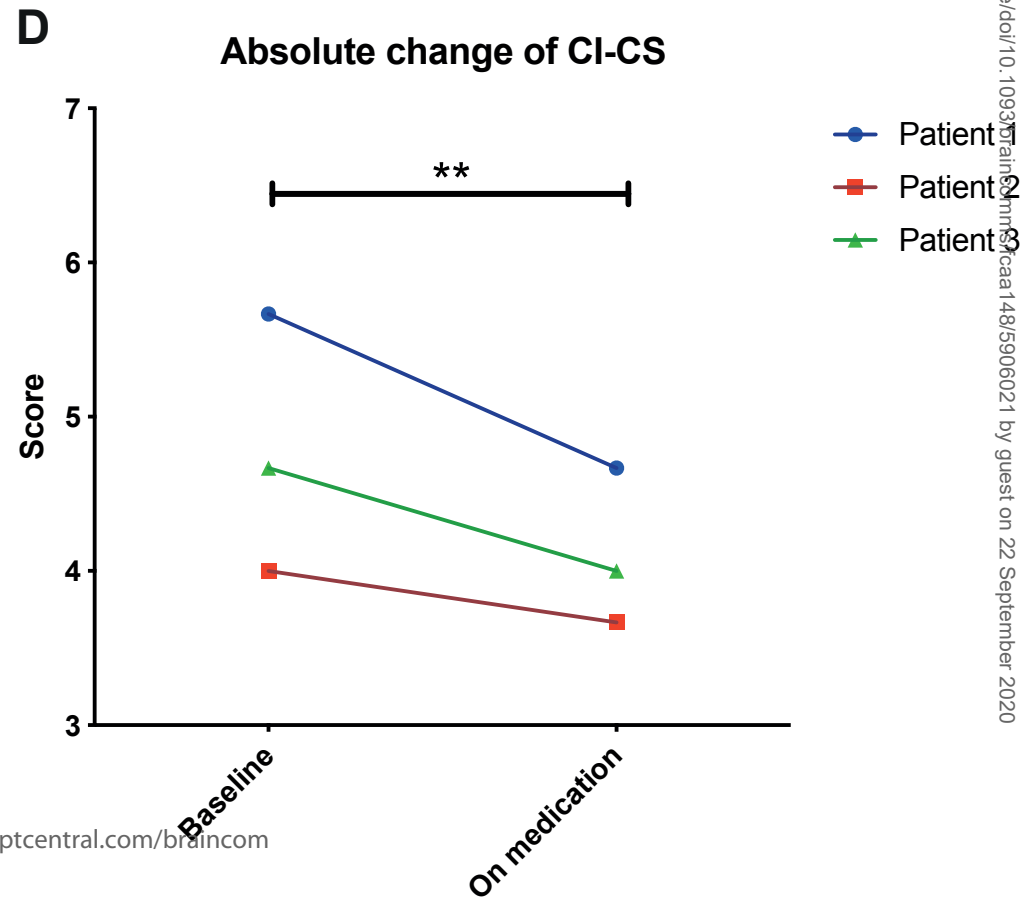
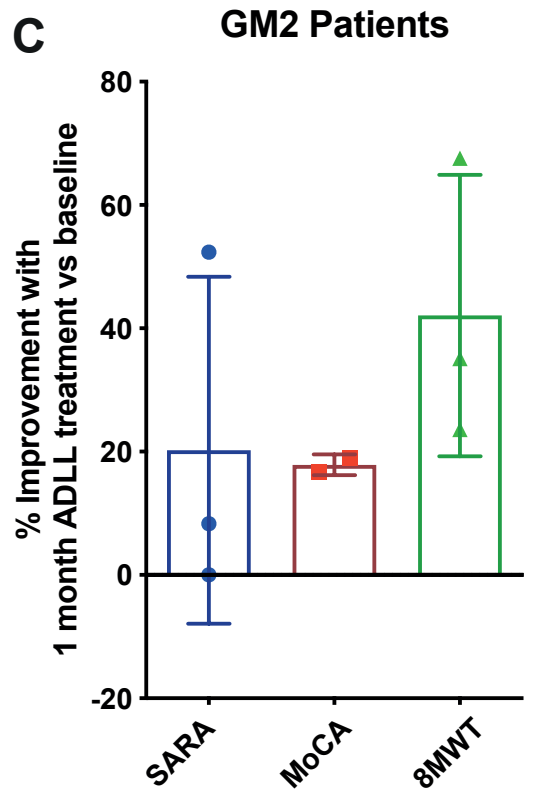
C



Murine studies

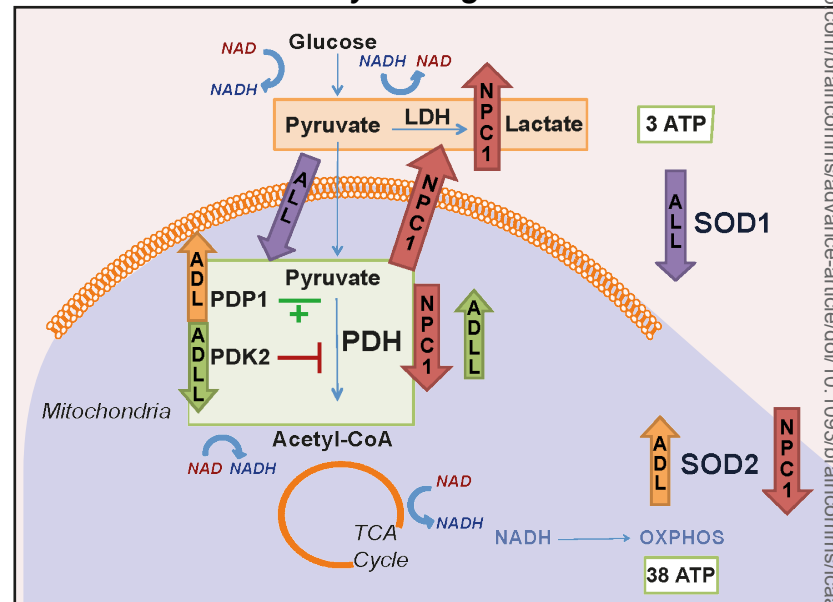


Clinical findings



Parameters	<i>Npc</i> ^{+/+} UT	<i>Npc</i> ^{-/-} UT	<i>Npc</i> ^{-/-} ADLL	<i>Npc</i> ^{-/-} ALL	<i>Npc</i> ^{-/-} ADL
Gait parameters					
Gait variation/Acute	0	↑	↓	↓	↓
Gait variation/Chronic	0	↑	↓	↓	↓
Duty cycle	0	↑	↓	↓	
Stand mean	0	↑	↓	↓	
Motor function	0	↓	↑	↑	
Biochemistry					
Brain					
GSL	0	↑		↓	
Sphingosine	0	↑			
Sphinganine	0	↑	↓		↓
Cerebellum					
GSL	0	↑	↓	↓↓	
Sphingosine	0	↑			↑
Sphinganine	0	↑			↓
Purkinje cell count	0	↓	↑		
CD68 density	0	↑		↓	
Liver					
GSL	0	↑	↓	↓↓	↓
Sphingosine	0	↑	↓	↓	↓
Sphinganine	0	↑	↓	↓	↓
Cholesterol	0	↑	↓	↓	↓
In vitro (CHO)					
Acidic volume/storage	0	↑	↓	↓	↓
Mitochondrial volume	0	↑	↓	↓	↓
Mitochondrial ROS	0	↑	↓	↓	↓
Survival	0	↓	↑	↑	

Cerebellum at 59 days of age








Neurological Domains	Improved	Stable	Deteriorated
Eye movement	8	4	1
Ambulation	8	4	1
Speech	3	7	3
Swallow	10	2	1
Fine motor skills	8	3	2
Cognition	6	6	1
Memory	10	2	1

Table 1 Number of patients (total cohort n=13) that improved, stabilised or deteriorated following ADLL treatment stratified by the neurological domains scored (NIH NCSS).

Examiner Number	Patient 1 Baseline	Patient 1 Treated	Patient 2 Baseline	Patient 2 Treated	Patient 3 Baseline	Patient 3 Treated	Paired t-test
1	5	4	3	3	3	3	
2	6	5	4	3	5	4	
3	6	5	5	5	6	5	
Mean	5.67	4.67	4	3.67	4.67	4	$p=0.0039$

Table 2. Blinded scoring of GM2 gangliosidosis patient videos pre and post ADLL treatment.

CI-CS Skala Clinical Impression of Change in Severity 1=normal, not at all ill; 2=borderline ill; 3=mildly ill; 4=moderately ill; 5=markedly ill; 6=severely ill; 7=among the most extremely ill patients

Niemann-Pick Type C1 <i>Acetyl-Leucine treatments</i>	GM2 Gangliosidosis <i>Acetyl-DL-Leucine treatment</i>
 <p>Niemann-Pick Type C1 Chinese Hamster Ovary cells (1mM Acetyl-leucine)</p> <ul style="list-style-type: none"> ✓ Reduced mitochondrial reactive oxygen species ✓ Reduced lysosomal volume ✓ Reduced lipid storage 	<p>Hexb^{-/-} mouse (0.1g/kg/day)</p>  <ul style="list-style-type: none"> ✓ Improved gait parameters
<p>Npc1^{-/-} mouse (0.1g/kg/day Acetyl-Leucine)</p>  <ul style="list-style-type: none"> ✓ Acute ataxia relief ✓ Differential effects and mechanism with enantiomers ✓ Miglustat synergy with Acetyl-DL-Leucine 	<p>GM2 patients (5g/day)</p>  <ul style="list-style-type: none"> ✓ Improved gait ✓ Improved Clinical Impression of Change in Severity
 <p>Niemann-Pick Type C patients (5g/day Acetyl-DL-Leucine)</p> <ul style="list-style-type: none"> ✓ Slowed disease progression (Annual Severity Increment Scores) ✓ Stabilisation or improvement in multiple neurological domains 	

Graphical abstract

254x190mm (72 x 72 DPI)

Abbreviated Summary:

This study investigates the disease-modifying effect of acetyl-DL-leucine in two neurodegenerative lysosomal storage diseases with different aetiologies: Niemann-Pick type C and GM2 gangliosidosis in both murine models and clinical studies. Acetyl-DL-leucine and its L enantiomer provide neuroprotection likely by altering metabolism – a new therapeutic approach for these diseases.